CSIRO EARTH SCIENCE AND RESOURCE ENGENEERING
www.csiro.au

Fault seal first-order analysis – SW Hub

Structural analysis for CO_2 containment risk for the SW Hub, Western Australia

Laurent Langhi, Bozkurt Ciftci, Julian Strand
Report EP13879
8 May 2013

ANLEC R&D
Unit 1.1, Level 1, NFF House, 14-16 Brisbane Avenue BARTON 2600

Citation

Langhi, L., Ciftci, B., Strand, J. (2013). Fault seal first-order analysis –SW Hub. CSIRO, Australia.

Copyright and disclaimer

Important disclaimer

Contents

Figures

Tables

Acknowledgments

The authors would like to acknowledge contributions to the South-West Hub Flagship project by the Western Australian Department of Mines and Petroleum (including the Geological Survey of Western Australia), the Western Australian Royalty for Regions Program and the Commonwealth Department of Resources, Energy and Tourism. The authors wish to also acknowledge financial assistance provided through Australian National Low Emissions Coal Research and Development (ANLEC R&D). ANLEC R&D is supported by Australian Coal Association Low Emissions Technology Limited and the Australian Government through the Clean Energy Initiative.

We thank Andy Nicol, James Underschultz and Sandeep Sharma for their constructive comments that improved the original report.

Executive summary

The Mandurah Terrace in the onshore central Perth Basin has been proposed as an environmentally suitable site for CO_2 injection (i.e. the SW Hub) with the "storage complex" reservoir, primary and secondary seal represented by the Triassic lower Lesueur Sandstone (Wonnerup Member), the Late Triassic upper Lesueur Sandstone (Yalgorup Member) and the Early Jurassic basal Eneabba Formation, respectively.

Prior investigations in the SW Hub region indicate that fault systems affect the target CO_2 storage reservoir and the potential top seals and it is known that changes in the pore pressure and stress field induced by fluid injection could alter the initial seal performance of a reservoir by either overcoming the faults membrane seal capacity leading to across- or along-fault circulation of CO_2 or by triggering slip on pre-existing faults leading to the potential along-fault circulation of CO_2.

This project is integrated with others ANLEC R&D funded projects. It uses stress data from the project *Advanced geophysical data analysis at Harvey-1: storage site characterization and stability assessment* (Pevzner et al., 2013), it uses facies and rock properties defined in the project *Facies-based rock proprieties distribution along Harvey-1 stratigraphic well* (Delle Piane et al., 2013) and it uses 3D facies models from the project *Stratigraphic forward modelling for South West Collie Hub Phase One - Static Model* (Griffith et al., 2012).

This project (*Integration of data from Harvey-1 well to support decision,* 7-1111-0201) relies on the available subsurface data and carries out a first-order assessment of the CO_2 containment potential for the SW Hub. A new geological model consistent with the integration of the latest 2D seismic reflection survey with the vintage seismic surveys and available geophysical data has been built. It integrates five stratigraphic horizons tied to formation tops in the new Harvey-1 data well (Neocomian UC, top basal Eneabba Shale, top Yalgorup, top Wonnerup and top Sabina sandstone) and 13 main faults that can be correlated between at least two 2D-seismic lines that show constancy in dip, strike orientation and offset. This represents a first-order geological model and the acquisition of additional seismic and well data is critical to reduce remaining geological uncertainty and further constrain the structural framework.

The membrane fault seal capacity has been assessed using the Shale Gouge Ratio (SGR) predictive algorithm that can be calibrated to derive an across-fault-seal failure envelop and to calculate a maximum fluid column height capable to be trapped by a fault without leaking. Three across-fault CO_2 migration scenarios are investigated: (1) between two self juxtaposed Wonnerup Members, (2) between the Wonnerup Member and a juxtaposed thief zone in the Yalgorup Member and (3) between the Wonnerup Member and the Eneabba Formation lying above the Yalgorup Member. The likelihood of lateral migration of CO_2 across faults between the Wonnerup Member and any interbedded sandstone thief zone in the Yalgorup Member can be locally high to the south of the SW Hub (faults F1, F11 and 14). The likelihood of lateral migration of CO_2 across faults within the Wonnerup Member can also be locally high to the south of the SW Hub with potential of westward migration beyond F1 if the CO_2 column exceeds the local offset. One fault (F10) juxtaposes the Wonnerup with the overburden Eneabba; however SGR values on the fault plane suggest an "average to low" likelihood of across-fault migration and the supported CO_2 column before breaching the membrane seal is between 110 and 1100m.

The relationship between the modelled faults and the present-day stress field has been investigated to define critically stressed fault segments most at risk of reactivation and failure with pore-pressure build-up due to injection. It is assumed that a reactivated fault will be associated with an increase in structural permeability (i.e., along-fault flow). The slip tendency values are minimum for faults striking parallel to SHmax and Shmin (105° and 195° respectively) and increase for strike orientation 50°-80° (SW-NE) and 130°-160° (SSE-NNW). However the slip tendency magnitude for the SSE-NNW-oriented faults in the SW Hub are low (typically between 0.15 and 0.3) suggesting a low risk of fault failure under the present-day stress. The critical pore pressure perturbation required to induce failure on any particular fault orientation is primarily depth-dependent as a result of an increase in depth resulting in an increase in stresses. This will

have the effect of preventing failure to occur. Therefore the smallest critical pore pressure perturbations required to reach failure stress are located to the north of the SW Hub along faults F1, F2 and F10 and once converted to an equivalent of CO_2 column height represent 1200 m or 1000 m of CO_2 column. However this corresponds to fracture stability values slightly <10MPa and empirical data from the Timor Sea suggest that below 10 MPa faults have a higher likelihood of experiencing onset of reactivation and leakage of hydrocarbons over geological times.

The cumulative frequency distribution of fault throws suggests that the geological model underestimates the number of faults with throw smaller than 120 m. A first-order fracture modelling suggests dominant shear failures with a maximum density of fractures in the central and eastern part of the SW Hub, adjacent to fault F10. The stress state of these small faults and fractures suggests that there is an average-low likelihood of failure under the present-day in-situ stress field. However the pore pressure increase required to reach failure stress decreases down to <10MPa to the west of the SW Hub where the Wonnerup and Yalgorup Members are the shallowest.

In light of the first-order assessment at the CO_2 containment for the SW Hub it is recommended to (1) acquire additional subsurface data, especially seismic reflection data in order to decrease uncertainties on the subsurface architecture and constrain the structural framework; (2) constrain the local stratigraphic framework by acquiring additional data to calibrate the V_{sh} models and the distribution of geomechanical and petrophysical properties; (3) acquire pressure data from within multiple fault compartments to constrain the across-fault pressure difference and calibrate the membrane fault seal calculations; and eventually (4) sample fault zones and define the geomechanical and petrophysical properties of faults to constrain the geomechanical fault seal assessment.

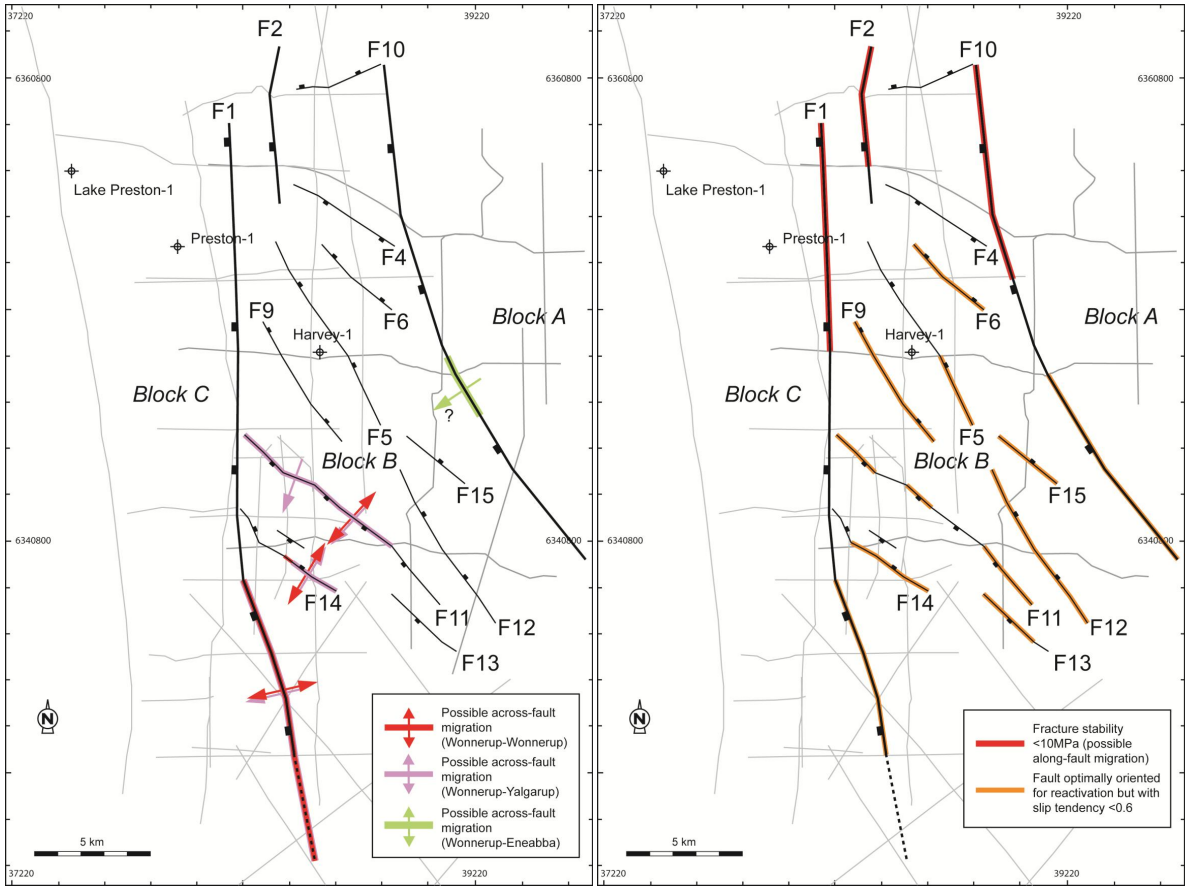

Summary of across-fault (left) and along fault (right) CO_2 migration potential for the SW Hub.

1 Introduction

The Perth Basin (Figure 1) was originally proposed by the APCRC's GEODISC Project during the regional assessment (e.g., Bradshaw and Rigg, 2001), as an environmentally suitable site for CO_2 injection. Subsequently the decision was made to proceed with a comprehensive site assessment and geological modelling of the Mandurah Terrace. This site was selected due to (i) the proximity to major CO_2 emission sources and (ii) the presence of a potentially suitable reservoir (Triassic Wonnerup Sandstone) and primary and secondary seals (Late Triassic Yalgorup intraformational shale and Early Jurassic basal Eneabba shale)(Figure 2, Causebrook et al., 2006; Varma et al. 2009). This is referred to the Collie Southwest CO_2 Geosequestration Hub or SW Hub hereafter (Figure 1). In February 2012 the Harvey-1 stratigraphic hole was drilled (2945 m) in order to determine the local stratigraphy (Figure 1). The Wonnerup and the Yalgorup Members were thoroughly investigated based on wireline logs interpretation and the geological and petrophysical characterisation of 6 cored sections totalling 217 m in length (Delle Piane et al., 2013).

Available seismic reflection data for the SW Hub clearly indicates that multiscale faults (10s of m to 10s of km) affect the target CO_2 storage reservoir (Wonnerup Member) and the potential top seals (Yalgorup Member and basal Eneabba Formation). Globally, there have been many examples of seismicity apparently induced by fluid injection in oil fields (see the review by Grasso, 1992) and it is known that changes in the pore pressure and stress field cause by fluid injection could alter the initial seal of a reservoir by either (1) overcoming the fault(s) membrane seal capacity leading to circulation of CO_2 by migration across or along the fault (e.g., Bretan et al., 2011; Ciftci et al., 2012), (2) by triggering slip on pre-existing fault(s) delimiting trap(s) or within the caprock leading to the potential loss of CO_2 by migration up the fault (e.g., Streit and Hillis 2004; Rutqvist et al. 2007; Chiaramonte et al. 2008; Bretan et al., 2011) or (3) by hydraulically fracturing the caprock (e.g., Secor, 1965, 1969).

For the purpose of assessing the first-order containment potential for the SW Hub, we investigate the first two points above related to faults that predate any CO_2 injection.

The containment assessment initially relies on the seismic mapping of the subsurface for the SW Hub, the definition of the main stratigraphic and structural elements and the development of a geological model consistent with the integration of a recently acquired (2011) 2-D seismic survey with the vintage seismic surveys and available geophysical data. Facies models capturing the 3D distribution of shale are constructed based on the Harvey-1 well data and 3D forward stratigraphic models carried out over the study area (Griffith et al., 2012).

In case of juxtaposition of the Wonnerup Member against another aquifer across a fault, the membrane (or capillary) seal (Jennings, 1987; Watts, 1987) is assessed using the Shale Gouge Ratio (SGR) predictive algorithm (Yielding et al., 1997; Freeman et al., 1998) that is considered as a proxy of up-scaled fault-rock composition (Bretan et a., 2011). Empirical calibration is used to derive a fault-seal failure envelop and to calculate a maximum fluid column height able to be trapped by a fault without leaking (Yielding, 2002; Bretan et al., 2003). Ciftci et al. (2012) demonstrate that SGR calculated on faults intersecting, but not offsetting completely, a caprock can also be used to qualitatively assess along-fault hydrocarbon migration potential and caprock bypass.

The effects of stress field changes on fault kinematic behaviour also needs to be understood, and fault reactivation potential should be estimated before CO_2 injection. Therefore the relationship between the modelled faults and the present-day stress field is investigated to define which critically stressed fault segments are most likely to be forced into failure with pore-pressure build-up. Areas of fault reactivation are associated with an increase in structural permeability and therefore with the potential for along-fault flow (Ferril et al., 1999, Mildren et al, 2005, Bretan et al., 2011).

Finally elastic dislocation theory (Okada, 1985; 1992; Dee et al., 2007) is used to predict the spatial distribution, orientation and mode of sub-seismic fractures in the Wonnerup and the Yalgorup Members

and assess their relative likelihood of reactivation under the present-day stress field and the impact of pore-pressure increase due to CO_2 injection.

This work led to an initial assessment of containment capacity for the SW Hub and is used to define data gap that need to be addressed in order to (1) fully characterise the impact of faults and fractures on the potential migration pathways of injected supercritical CO_2 and (2) select the most optimal test injection site(s); and (3) design an effective measurement, monitoring and verification strategy.

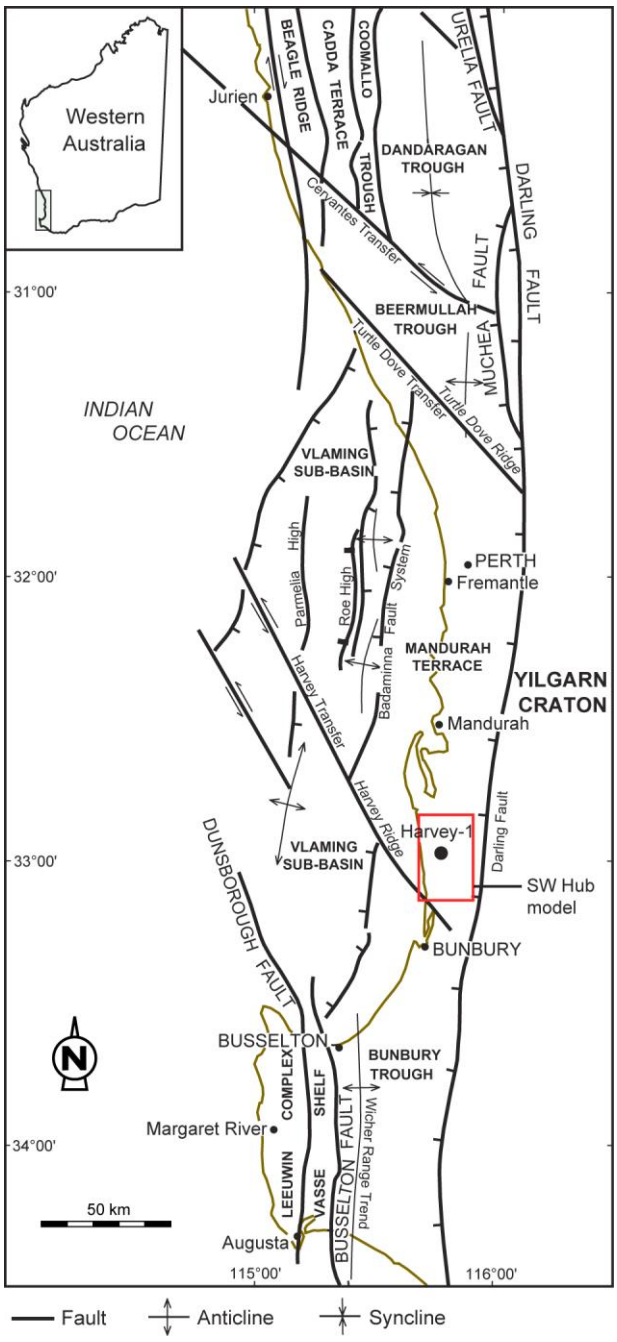

Figure 1: Perth Basin subdivision, tectonic lineaments and location of the SW Hub model. Modified form Crostella and Backhouse, 2000.

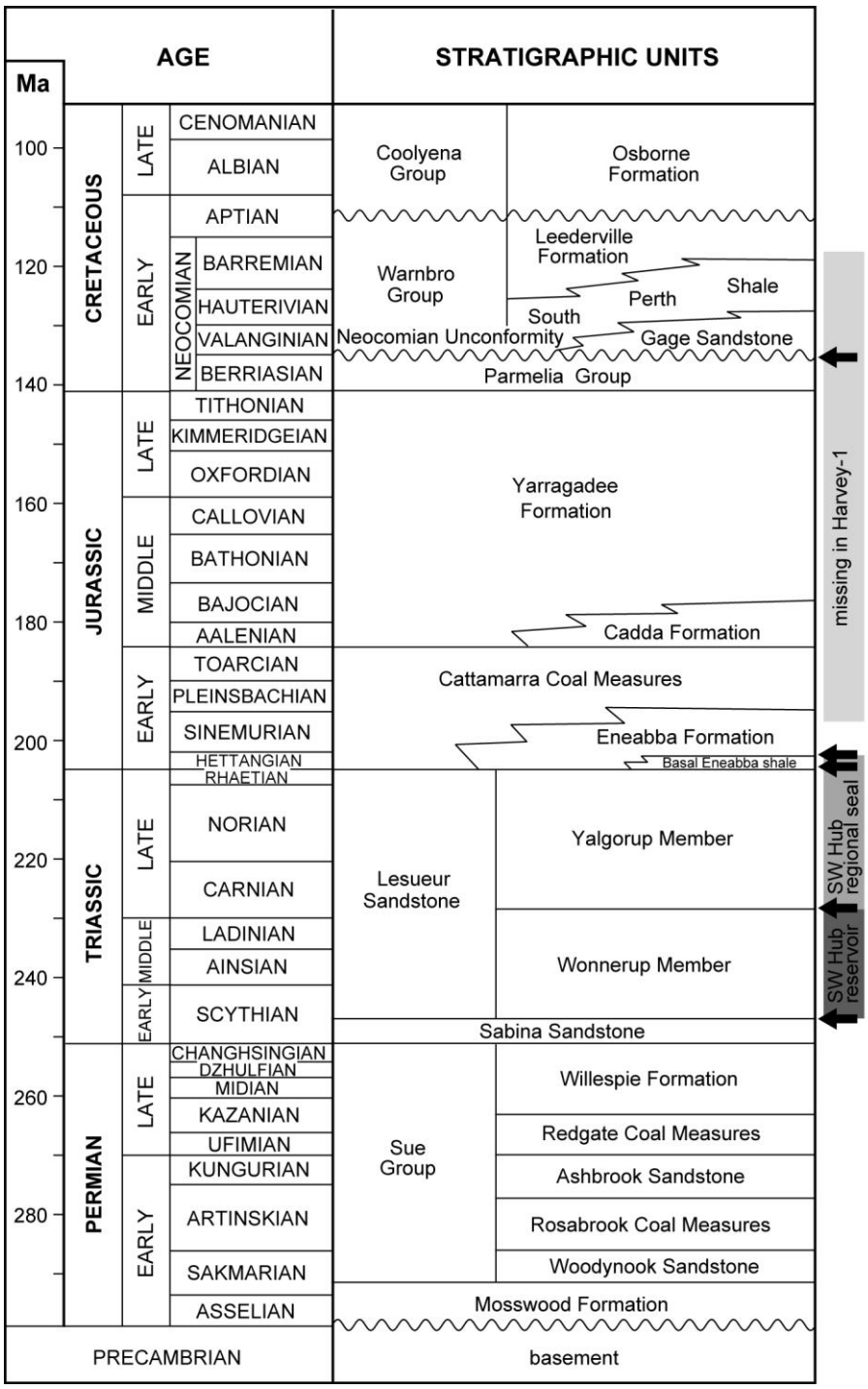

Figure 2: Stratigraphy of the central and southern Perth Basin and definition of the proposed CO_2 containment reservoir and top seal for the SW Hub. Modified form Crostella and Backhouse, 2000. The arrows indicate the mapped seismic horizons.

2 Geological setting

The study area is located in the central part of the onshore Perth Basin, at the south end of the Mandurah Terrace (Figure 1, Crostella and Backhouse, 2000), approximately between latitudes 32˚50' and 33˚10'. To date, only limited drilling has been carried out in the southern Mandurah Terrace and its structural setting is still not well understood because of the sparse and poor quality seismic reflection data. The Mandurah Terrace forms a terrace in comparison to the offshore Vlaming Sub-basin to the west and is bounded to the east by the Darling Fault System. To the south the Mandurah Terrace is bounded by the Harvey Ridge that is a broad (> 10km) NW-trending basement high associated with normal and strike-slip deformation in the Phanerozoic sedimentary cover (G. Bernardel, pers. comm., 2012). Both the Darling Fault System and the Badaminna Fault bounding the terrace to the east and west, respectively, trend to the N-NNE. The structural pattern for the southern Mandurah Terrace primarily shows NNE to NNW trending features (Cockbain, 1990; Crostella and Backhouse, 2000). Based on interpretation of regional gravity data, Wilkes et al. (2011) and Iasky and Lockwood (2004) suggest the presence of NNW to NW trending features in the southern Mandurah Terrace and to the south, respectively (Figure 3). NNW trending structures are also widespread in the western part of the Yilgarn Craton east of the Mandurah Terrace (Myers and Hocking, 1998; Wilkes et al., 2011) where they form, for instance, the bounding faults of the intra cratonic Collie Basin.

Crostella and Backhouse (2000) detailed the stratigraphy of the central Perth Basin. On the southern Mandurah Terrace (Figure 2) the oldest known sedimentary rocks are Permian in age and belong to the Sue Group. The Lake Preston-1 well intersects c. 150m of Late Permian Willespie Formation. However, well correlation suggests that older Permian sediments are present in the study area (Crostella and Backhouse, 2000). The Sabina Sandstone overlies the Willespie Formation with an apparently conformable contact, and is conformably overlain by the Lesueur Sandstone. The Lake Preston-1 well intersects a complete c. 500m section of Sabina Sandstone while the recently drilled Harvey-1 well intersects only the upper 50m (2895mDRT to 2945mDRT). The units intersected in Harvey-1 have been investigated by Delle Piane et al. (2013) and are listed in Table 1. The 1515m of Wonnerup Member (lower Lesueur Sandstone) drilled in Harvey-1 well consists primarily of interbedded coarse to gravelly sandstones occasionally punctuated by fine to medium, cross-laminated sandstones and massive, coarse-grained to gravelly sandstones and mudstone layers typical of fluvial environments. The Yalgorup Member (upper Lesueur Sandstone) is 676m thick in Harvey-1 well and represents an interbedded succession of mixed coarse to gravelly facies and fine to medium grained facies and siltstones and mudstone. Open, gently inclined, fractures often occur as conjugate sets, exhibiting prominent slickenlines. A 79m thick basal Eneabba Shale is interpreted in Harvey-1 well using correlation from other wells and through breaks on the induction-electrical, gamma-ray and sonic logs. Although the residual trapping is expected as the sealing mechanism, the Yalgorup Member and Eneabba basal Shale are believed to represent potential physical top seals for the reservoirs in the Wonnerup Member. The basal Eneabba Shale is overlain by 375m of the Eneabba Formation. No core was recovered from the Eneabba Formation in Harvey-1; however Mory and Iasky (1996) described it as a fluvial coarse to very coarse grained sandstone interbedded with local minor conglomerate, and multicoloured claystone and siltstone. The Early Jurassic Eneabba Formation is eroded and overlain by the Neocomian Unconformity. Based on well data from the Bunbury Trough to the south and the Beermullah Trough to the north (Crostella and Backhouse, 2000) and vitrinite reflectance data (Iasky, 1993) we estimate that at least 1500m of Early to Late Jurassic sediment might have been deposited on the southern Mandurah Terrace and then eroded during the Neocomian (i.e. Berriasian-Valanginian). The unconformity is overlain by 215m of Early Cretaceous Leederville Formation described as a sandstone, shale, and conglomerate interval in the Leederville Valley waterbore (Fairbridge, 1953). There is 29m of Guilford formation are present above the Leederville Formation in Harvey-1.

Tectonic evolution of the central Perth Basin is described in Cockbain (1990) Crostella and Backhouse (2000) or Iasky and Lockwood (2004). During the Late Carboniferous to Early Permian, north-trending

regional rifting marked the beginning of sedimentation within the Mandurah Terrace (Crostella and Backhouse, 2000). During the Permian, Triassic, and Jurassic, the Darling Fault System acted as a growth fault, which resulted in Permian to Neocomian clastic sedimentation from the emergent Yilgarn Craton that thickens toward the fault. During the Late Jurassic to Early Cretaceous the onshore part of the Perth Basin was uplifted, with limited and/or discontinuous deposition, and by the Neocomian the final separation of Australia from India produced intense deformation, uplift and erosion (Neocomian Unconformity). This episode is responsible for the bulk of the deformation observed in the study area. Although fault movement drastically decreases after the Neocomian break-up, localised fault activity is possible due to differential compaction or Cretaceous and/or Tertiary stress regime.

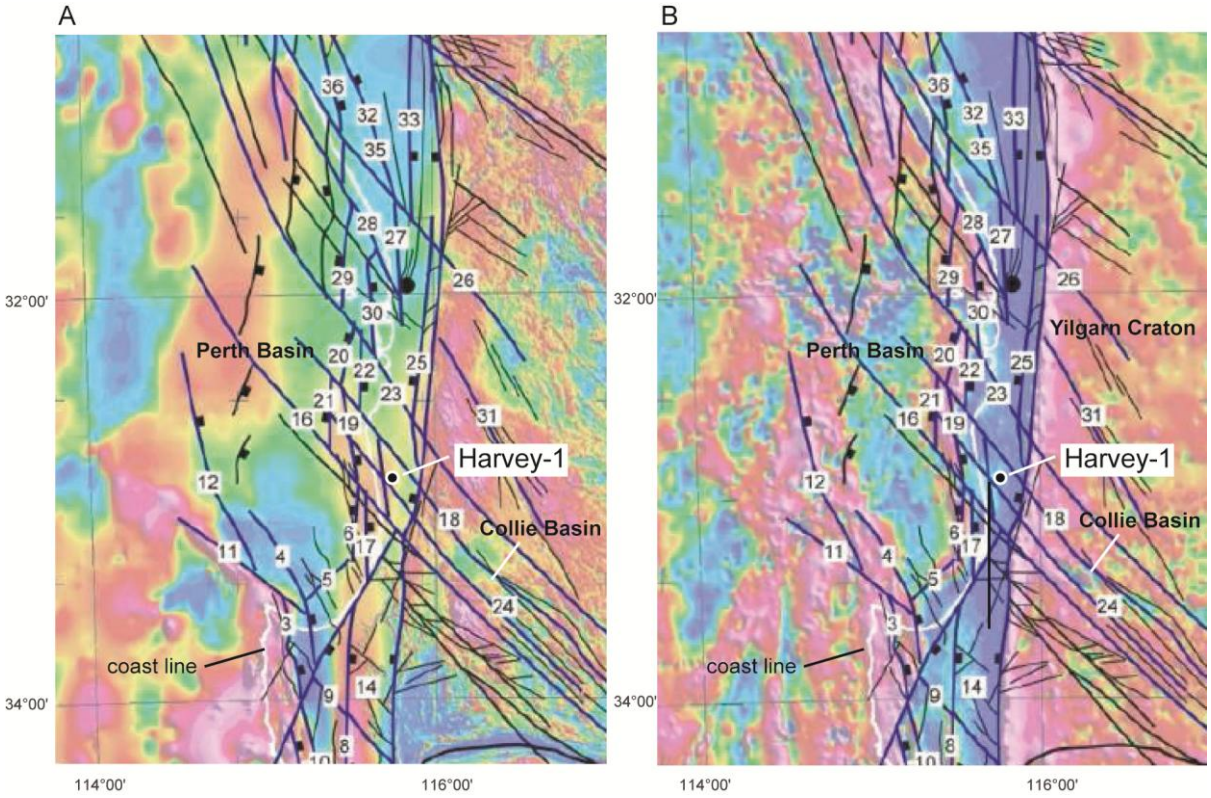

Figure 3: Regional geophysical data showing some major structural trends. A) Reduced pole to aeromagnetic image. B) Vertical gradient of isostatic residual gravity. Modified form Wilkes et al., 2011.

STRATIGRAPHIC UNIT	TOP MDRT	TOP TVDSS
Guildford	5	+20
Leederville	36	-11
Eneabba	250	-225
Basal Eneabba shale	625	-600
Yalgorup	704	-679
Wonnerup	1380	-1335
Sabina	2895	-2870
Total depth	2945	-2920

Table 1: Harvey-1 well; formation tops.

3 Geological model

The modelled area represents a box of c. 20 km by 30 km around the Harvey-1 well (Figure 4). The model extends to the coastline in the west and the Darling Fault in the east. The final model includes the main faults (correlated over at least two 2D-seismic lines) and five stratigraphic horizons, i.e. the Neocomian Unconformity, the top basal Eneabba Shale, the top Lesueur Formation (top Yalgorup Member), the top Wonnerup Member and the top Sabina Formation (Figure 2). The horizons are tied to the top formation markers from Harvey-1 (Table 1).

3.1 Dataset

Mapping of the 2D-seismic reflection data for the SW Hub has been carried out to define a consistent geological model. Various vintages of seismic reflection data were integrated in order to optimise the line spacing. The model was initially constructed around the 2011 2D GA Lower Lesueur seismic survey as these data present the best resolution and signal to noise ratio and Harvey-1 lies less than 60m from line 11GA_2 (Figure 4). The 2011 2D GA Lower Lesueur seismic survey includes 6 lines for a total length of c. 100km with individual lines between 10km to 26km (Figure 4). The CDP interval is 12.5m and the record length is 5sec (TWT). Three lines are trending N-S to SSW-NNE and three lines are trending E-W to ESE-WNW.

Five additional 2D-seismic surveys, shot between 1964 and 1981 and reprocessed in 1990, were used to extend the data coverage and the line density. This represents a total of 29 lines for approximately 350 km. These vintage lines generally have a record length up to 5sec (TWT) and are generally N-S or E-W trending (Figure 4).

The seismic line spacing over the study area is between 1km and 5km with an average spacing of 3km. Although this coverage is sufficient to highlight the general trend of the stratigraphic horizons it is insufficient to accurately define medium to small scale structures (<2km) and to unambiguously define the structural pattern and correlate faults between lines. This limitation increases uncertainties related to fault connectivity, fault offset distribution or fault size and density.

Regional gravity and magnetic data for the central Perth Basin from Wilkes et al. (2011) and from the southern Perth Basin and the south part of the Vlaming from Iasky and Lockwood (2004) were used to constrain the regional orientation of the structural trends (Figure 3). The resolution of the gravity and magnetic data over the study area does not allow an accurate and unambiguous structural interpretation.

Subsurface interpretation from 2D-seismic reflection data from the Vlaming Sub-basin (Figure 5, Causebrook et al., 2006; Nicholson et al., 2008) was used to define the offshore fault pattern and constrain the structural orientation of the study area.

Outcrop data from Le Blanc Smith (1993) in the Collie Basin were used to constrain the regional orientation of faults in the western Yilgarn Craton and the Collie Basin.

Figure 4: Modelled area for the SW Hub around Harvey-1. The 2011 2D GA Lower Lesueur seismic survey is in orange and vintage seismic lines are in yellow.

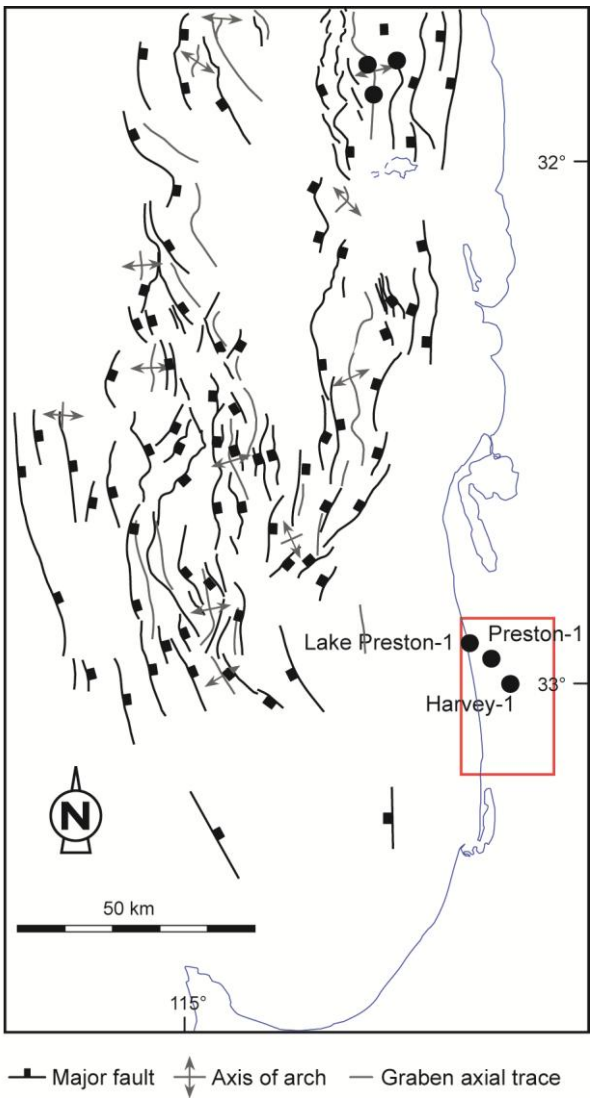

Figure 5: Offshore southern Perth Basin structural style. The red box represents the SW Hub model. Modified from Nicholson et al. (2008).

3.2 Harvey-1 time depth relationship

A 3D velocity model was built by defining a 3D grid comprising approximately 1,126,000 grid cells (200m x 200m bin) over 100 layers between 0 (seismic datum) and 5 seconds TWT. The grid was populated by using 187 pseudo-wells at each stacking location of the 2011 seismic survey with a velocity log derived from the post stack time migration (PSTM) stacking velocities. Linear interpolation of the PSTM velocities produced a 3D velocity model capturing the spatial variation of the velocity field. This model was then calibrated against a 1D velocity model derived from the Harvey-1 VSP data (Pevzner et al., 2013). The calibration accounted for the difference between the PSTM stacking velocities and the VSP velocity (i.e., true vertical propagation velocity) and achieved an adequate approximation of the seismic horizons to the well picks (Al-Chalabi, 1994; Etris et al., 2001). Accordingly, the model provided a satisfactory depth conversion with less than a 2.0 m vertical positioning error for the top Lesueur Sandstone at the location of Harvey-1. The error is 5.5 and 2.5 m for the top Basal Eneabba Shale and Wonnerup Member, respectively. We believe that this level of precision in depth conversion is sufficient for the purpose of the study.

3.3 Static model

The final static model comprises five stratigraphic horizons tied to formation tops in Harvey-1 (Figure 2 and 6):

- The Neocomian Unconformity (250mDRT in Harvey-1) coincides with a strong negative reflector at c. 210ms TWT. This interface is usually easily mappable as it represents an angular unconformity with the truncation of the Eneabba Formation. This horizon is usually not offset by faults.
- The top basal Eneabba Shale (625mDRT in Harvey-1) coincides with negative reflector of variable intensity at c. 480ms TWT. To date the interpretation of this horizon remains ambiguous due to the low contrast in acoustic impedance. Over the study area this horizon has been mapped as the second to third trough above the top Lesueur horizon (top Yalgorup).
- The top Lesueur (top Yalgorup, 704mDRT in Harvey-1) coincides with a positive reflector at c. 550ms TWT. The Yalgorup Member is characterised by a typical seismic facies with high reflectivity and average to high continuity.
- The top Wonnerup Member (1380mDRT in Harvey-1) coincides with a strong positive reflector at c. 980ms TWT. This reflector is usually easily mappable as it represents the interface between the reflective and continuous Yalgorup facies and the more transparent and chaotic Wonnerup facies.
- The top Sabina sandstone (2985mDRT in Harvey-1) coincides with a strong positive reflector at c. 1800ms TWT. This reflector represents the interface between the transparent Wonnerup Member and the more reflective and continuous Sabina sandstone and Sue Group.

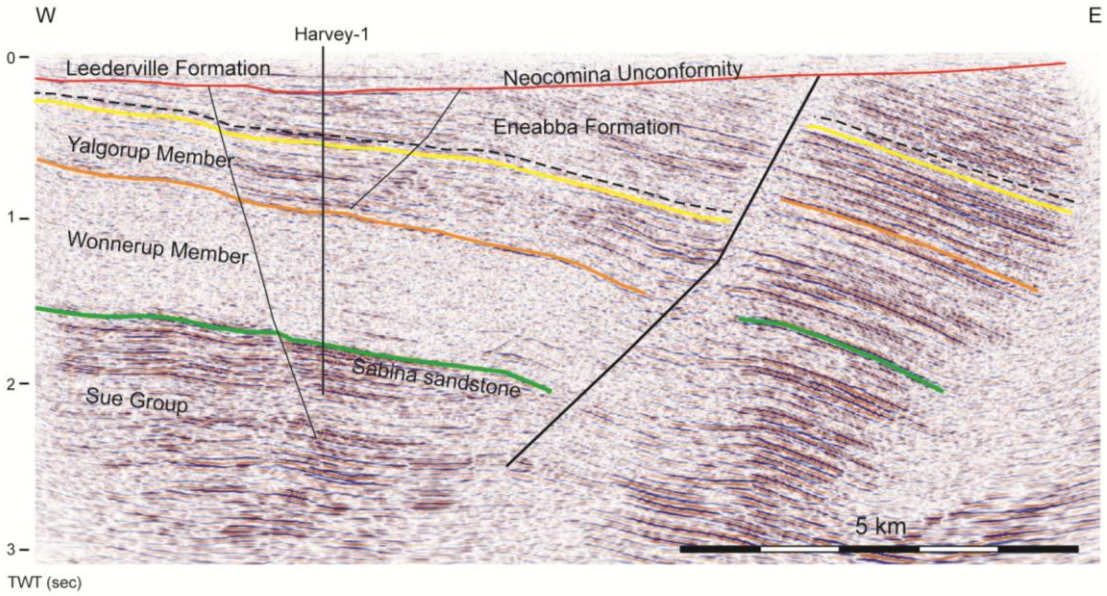

Figure 6: Seismic line 2011 2D GA L2 through Harvey-1 showing the mapped horizons. Location on Figure 4.

No clear seismic leakage indicators (e.g., gas chimney, amplitude anomaly, velocity effect) have been observed for the SW Hub. However as no significant shows of hydrocarbon have been recorded on the Mandurah Terrace, the absence of acoustic anomalies typical of hydrocarbon leakage (e.g. Cartwright et al., 2007) does not provide a positive confirmation that the faults are sealing.

In the study area, although tectonic strain occurred during the Jurassic, the main structural episode post dated the deposition of the Eneabba Formation and is mostly related to the Neocomian break-up between Australia and India. Important uncertainties remain for the detailed structural architecture over the study

area due to the low density and poor resolution of 2D-seismic reflection data. However a regional first-order geological model (Figure 7) consistent with the stratigraphic and structural interpretation and honouring regional data is proposed and used for the fault seal assessment and sub-seismic fracture prediction. It is anticipated that the current model will be updated once a new 3D seismic survey is acquired. The current model (Figure 7), including 13 main faults, is characterised by a main N-S fault to the west (F1 in Figure 7), parallel to the Darling Fault, a large NNW-SSE to N-S fault to the east (F10 in Figure 7) and a series of NW-SE to NNW-SSE faults in between. The NNW-SSE structural trend is consistent with those interpreted from gravity and aeromagnetic data and from outcrop in the Collie Basin (Le Blanc Smith, 1993; Iasky and Lockwood, 2004; Wilkes et al., 2011). The faults usually intersect the Mesozoic sedimentary succession and are truncated by the Neocomian Unconformity (Figure 6).

The two main faults oriented N-S (F1, Figure 7) and NNW-SSE to N-S (F10, Figure 7) present maximum modelled offsets of 900 and 1300 m, respectively, and define three fault blocks (Figure 7). Block “A” lies between the Darling Fault to the east and F10, Block “B” included Harvey-1 and lies between F1 and F10, and Block “C” lies west of F1 fault. Fault movement is interpreted on seismic reflection data as mostly normal with some local possible indications of strike-slip component (i.e. local pop-up structures and vertical faults segments). The faults dip in the model at around 60°. Lower angle faults are suggested to possibly exist on newly processed seismic (Shragge, J. and Lumley, D. personal comm.) but are not included in the present model due to the remaining uncertainties related to their strike orientation and size.

Variations of thickness in the Wonnerup Member (Figure 8A) suggest that the main faults were temporally active during the Early-Mid Triassic (around 400m for F1 and F10). The thickness of the Yalgorup Member and the basal Eneabba shale (Figure 8B) are much more constant suggesting low to nil tectonic activity during the Late Triassic to Early Jurassic. The majority of the displacement on the faults in the model post-dated the basal Eneabba shale deposition and pre-date the formation of the Neocomian Unconformity and are associated with the Neocomian break-up.

The faults present in the model are those that can be correlated between at least two 2D-seismic lines (compatible dip direction, strike orientation and displacement range). Several faults are interpreted on a single seismic profile and have not been included in the model due to too high uncertainties on strike orientation, size and displacement distribution. The future acquisition of additional seismic and well data would be critical to reduce uncertainty in the current structural model that included the majority of seismically resolvable faults.

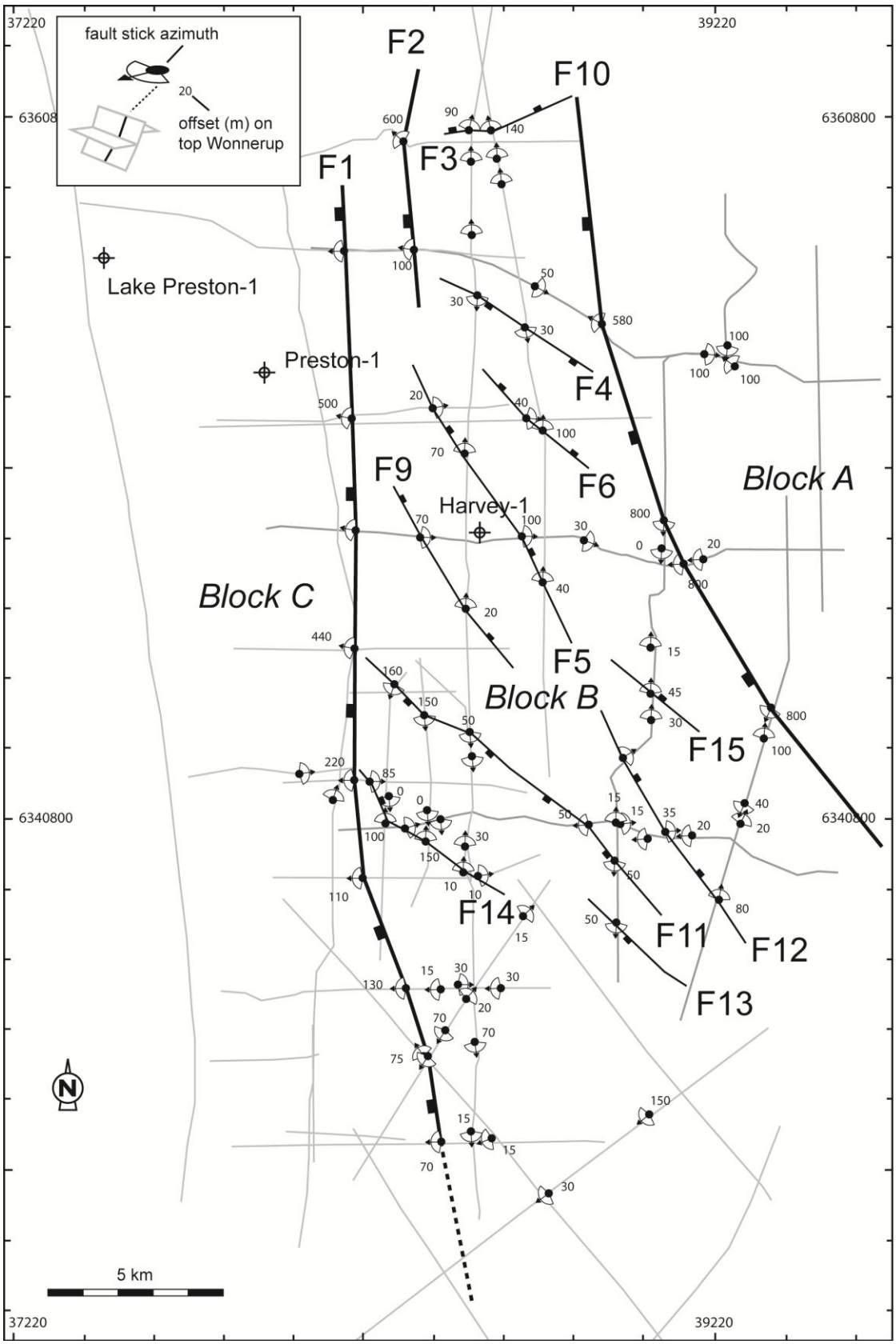

Figure 7: Modelled faults at the top Wonnerup. Fault stick azimuths (and range) interpreted on 2D-seismic lines and offset (m) on the top Wonnerup horizon are shown.

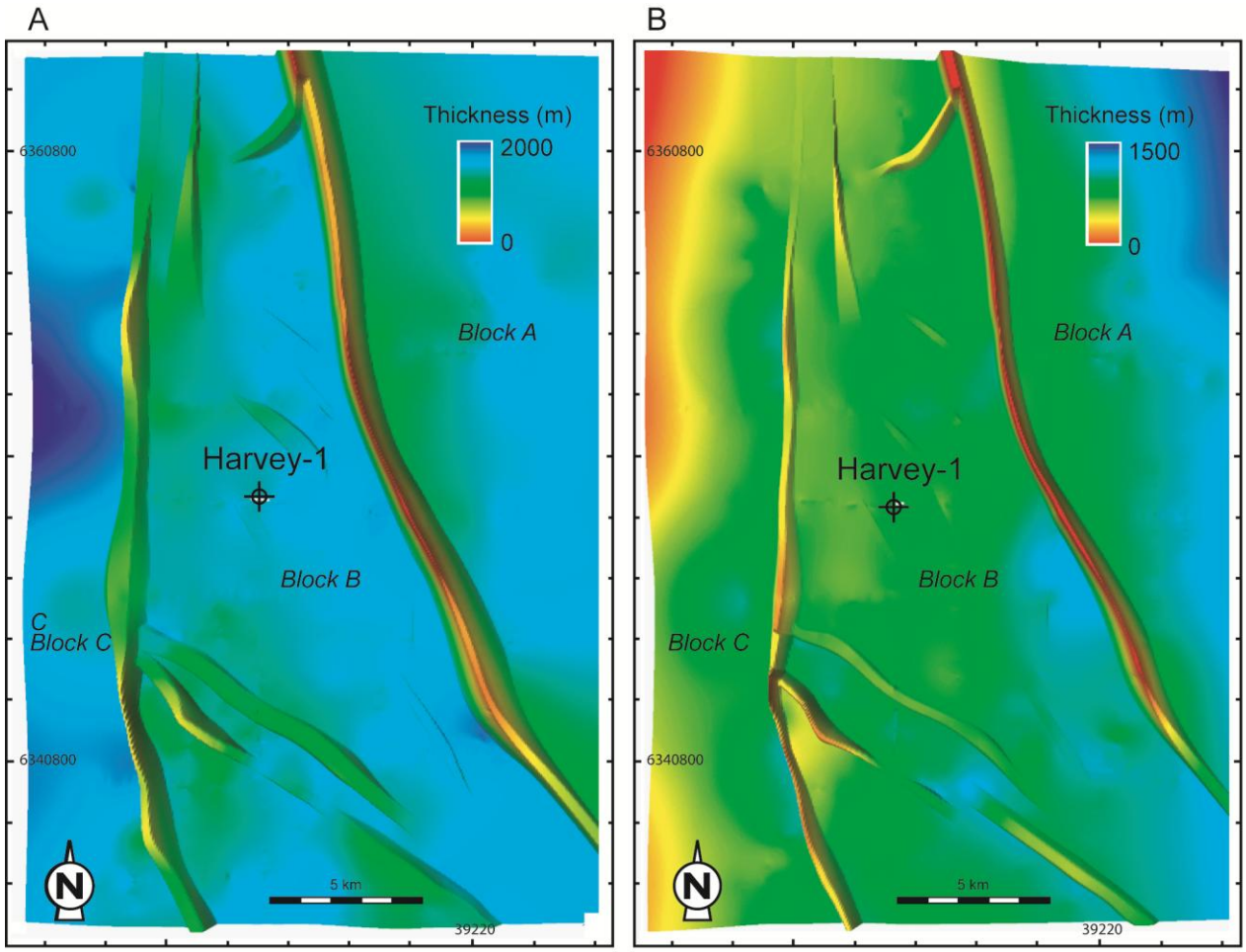

Figure 8: Thickness maps in the SW Hub. A) Wonnerup Member. B) Yalgorup Member.

4 Shale Volume

The distribution of the phyllosilicate content, or volume of shale (V_{sh}), represents a key factor in defining the membrane seal capacity of the faults (Knipe et al., 1997; Yielding, 1997; Sorkhabi and Tsuji, 2005; Underschultz, 2007) as it volumetrically relates to the shale gouge fraction of the fault rocks. Two 3D V_{sh} models for the SW Hub were constructed from (1) the inversion and up-scaling of the Harvey-1 gamma-ray log and (2) a net-to-gross derived from a multiscale stratigraphic forward model (Griffith et al., 2012).

4.1 Shale volume from Harvey-1 gamma-ray log

A V_{sh} can be derived from the Harvey-1 well gamma ray index (V_{sh}gamma hereafter), by using standard oilfield petrophysical methods (Asquith and Krygowski, 2004). The resulting V_{sh}gamma at the resolution of gamma ray log was up-scaled using an arithmetic mean to match with the vertical grid resolution of the 3D geological model. A layer-cake geology is assumed without any spatial variation in the same stratigraphic level and the well-derived V_{sh}gamma was extrapolated to the surrounding area (Figure 9A). Although this approach honours the data from Harvey-1, it simplifies the lateral distribution by ignoring the natural variation of the sedimentary depositional environment. Note that the main N-S fault (F1 in Figure 7) and N-S to NNW-SSE fault (F10 in Figure 7) are approximately 4 and 6 km away from the Harvey-1, respectively and a variation in facies is likely across such distances. Yet, this layer-cake distribution provides a potential solution among the infinite number of equally valid V_{sh} distributions that can be produced with the available data. Therefore, it could still provide a useful working model constraining the lithological character of the relevant sedimentary sequence.

Figure 10 shows the net-to-gross distribution over the SW Hub derived from the Harvey-1 gamma-ray log where net-to-gross value lower than 20% are displayed (high shale content). Shale-rich units (>80%) are all located above the Wonnerup Member. By definition the V_{sh}gamma model is continuous. The mean V_{sh} value is 37% for the Wonnerup Member and 50% for the Yalgorup Member.

4.2 Shale volume from forward stratigraphic modelling

A comprehensive process-based stratigraphic forward modelling package (Sedsim) was used to explore depositional concepts in the South Perth Basin by producing numerical stratigraphic forward models based on the current understanding of the basin's stratigraphy and depositional systems. The program models sediment erosion, transport and deposition, and predicts clastic and carbonate sediment distributions across a given bathymetric surface. In Sedsim the Navier-Stokes equations and the continuity equation are simplified and solved by using a marker-in-cell technique in two horizontal dimensions (Tetzlaff and Harbaugh, 1989). Past studies that have demonstrated the value of using Sedsim modelling include those by Griffiths et al. (2001), Li at el al. (2005), Griffiths and Dyt (2001), Griffiths and Paraschivoiu (1998), Koltermann and Gorelick (1992) and Martinez and Harbaugh (1993), Meyer et al (2011), Salles et al (2009, 2011a, 2011b).

For the SW Hub the model was run from 250 Ma to 182 Ma resulting in 850 output layers. Nested grids were used in the simulation with a larger extent, but coarser (5 km spacing), 75 x 40 km grid surrounding a 15 x 10 km finer (0.5 km spacing) grid covering the immediate study area near Harvey (Griffith et al., 2012). The main sediment input to the South Perth Basin and the SW Hub region during this period was via major rivers sourcing from the south from what is now Antarctica; the major emphasis in the models has been focussed on evaluating the source introducing material at the southern end of the model. Smaller scale streams entering the basin from the east were treated as simple sources remaining constant throughout the model. Griffith et al. (2012) give an extended description of the forward stratigraphic model. The outcome is the distribution of four granulometric classes (i.e., coarse sand, medium sand, fine sand and

mud) at each sample point. The three sand classes are assigned to the net and the mud class is assigned to the non-net and the 3D V_{sh} (V_{sh}sedsim hereafter) is constructed (Figure 9B) as the inverse of the net-to-gross.

Figure 10b shows the net-to-gross distribution over the SW Hub derived from the Sedsim model where net-to-gross value lower than 20% are displayed (high shale content). The shale distribution above the Wonnerup Member is widespread but forming discontinuous bodies of shale-rich material. The inferred regional top seal section including the Yalgorup Member and the basal Eneabba shale is captured by the model. Large shale-rich packages are predicted within the Wonnerup Member.

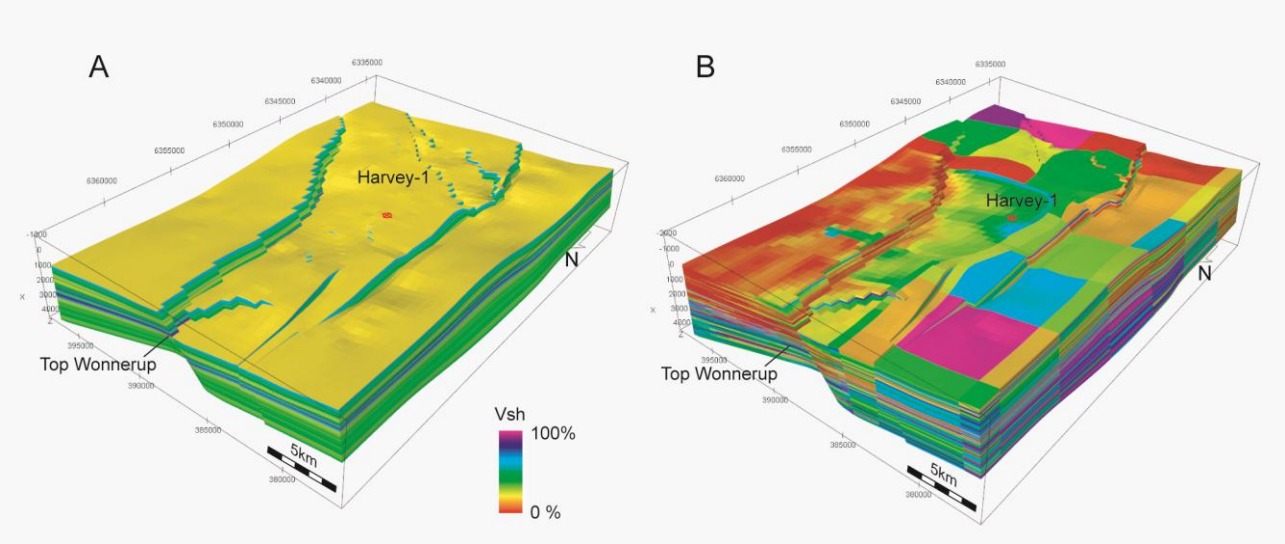

Figure 9: Volume of shale models (Vsh). A) Vsh derived from Harvey-1 gamma-ray log (Vshgamma). B) Vsh derived from forward stratigraphic model (Vshsedsim).

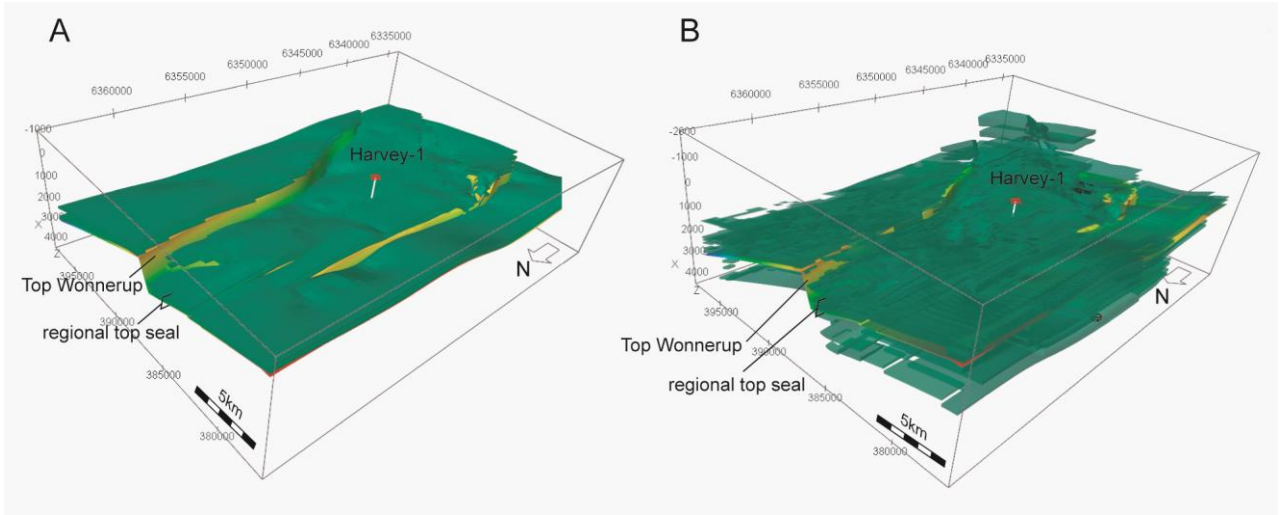

Figure 10: Net-to-gross (filtered) distribution. Only value lower than 20% are displayed (shale-rich part). A) Net-to-gross derived from Harvey-1 gamma-ray log. B) Net-to-gross derived from forward stratigraphic model.

5 Fault seal assessment

In order to assess whether the proposed SW Hub storage site for CO_2 is geologically stable over long time periods, it is critical to assess the sealing behaviour of the faults to injected CO_2 (e.g., Bretan et al., 2011).

- The evaluation of the membrane fault seal potential is used to predict if a fault acts as a sealing lateral barrier thus permitting CO_2 to accumulate within a trap.
- The modelling of the stress state on the fault planes is used to predict the likelihood of fault reactivation under the present-day stress regime and if increasing formation pressure generated either by a CO_2 column (capillary pressure) or injection, is likely to trigger fault instability, reactivation and along-fault migration.

5.1 Membrane fault seal potential

The juxtaposition pattern of the lithology is the predominant influence on membrane fault seal in clastic sequences. It has been well documented in recent years for many hydrocarbon fields globally (e.g. Bouvier et al. 1989; Jev et al. 1993; Childs et al. 1997; Fristad et al. 1997; Fulljames et al. 1997; Yielding et al. 1997; Knipe et al. 1998; Yielding 2002; Bretan et al. 2003). Large faults (seismic scale) offsetting reservoirs and shale-rich sealing units may form seal if they juxtapose reservoir rocks against sealing rocks (i.e., juxtaposition seal; Allan, 1989; Freeman et al., 1998; Yielding et al., 1997) or if the faulting process has generated a membrane seal, because of the presence of mechanically derived fault rock (i.e., gouge; Fisher and Knipe, 1998) that is of lower permeability and which impedes fluid flow (Bouvier et al., 1989; Knipe, 1992; Antonellini and Aydin, 1994; Gibson, 1994).

The generation of gouge is linked to the sliding of different lithologies past one another (Yielding et al. 1997). The first-order control on such fault-rock development is identified as the composition of the faulted lithologies and the amount of displacement on the fault (Fisher and Knipe, 1998). The capillary entry pressure of the fault-zone material is the critical parameter in determining whether a fault can successfully seal a non-wetting fluid accumulation (hydrocarbon or CO_2) when sands are juxtaposed. Leakage of hydrocarbons or CO_2 through the fault zone takes place when the difference in pressure between the water and hydrocarbon phases (buoyancy pressure) exceeds the pressure required for hydrocarbons or CO_2 to enter and pass through the largest interconnected pore throat in the seal (displacement or capillary entry pressure) (Bretan et al., 2003).

For the SW Hub the Shale Gouge Ratio (SGR) algorithm (Figure 11, Yielding et al., 1997; Freeman et al., 1998) is used to estimate the amount of phyllosilicates incorporated in the fault zones. A high SGR value is expected to correspond to more phyllosilicates in the fault zone (e.g. clay smear), and therefore to higher capillary threshold pressure and lower permeability (Bretan et al., 2011). Yielding (2002) observed that SGR>15–20% corresponds to faults that are sealing to hydrocarbons. A quantitative calibration of SGR against pressure difference data allows Yielding (2002) and Bretan et al. (2003) to derive a relationship between SGR and the maximum hydrocarbon column height supported by a fault:

$$h_{max} = 10^{(SGR/27-C)}/(\rho_w - \rho_h)g \quad (1)$$

where *C* is 0.5, 0.25, 0 for increasing burial depths (see Bretan et al. 2003 for details), ρ_w and ρ_h are the densities of water and hydrocarbon and *g* is the acceleration due to gravity. Bretan et al. (2011) demonstrate the application of this fault seal methodology in the context of CO_2 storage.

In the Block B (Figure 7), the Wonnerup Member juxtaposes against the Yalgorup Member and the basal Eneabba shale or against itself (Table 2). The SGR values for the juxtaposition seal (i.e., the upthrown Wonnerup Member is juxtaposed against the Yalgorup Member and Eneabba shale) for the large N-S faults

F1 and F10 vary from 40% to 80% using the V_{sh}gamma and from 13% to 90% using the V_{sh}sedsim (Figure 12). The modelled fault offsets on the top Wonnerup in the Block B range from 1300 to 50m (Figure 13). This means that a CO_2 column larger that 50m could potentially encounter the self-juxtaposition of the Wonnerup Member. The SGR values for the self-juxtaposition (i.e., the upthrown Wonnerup Member is juxtaposed against itself) vary from <20% to >45% using the V_{sh}sedsim and >35% using the V_{sh}gamma for fault F1. The SGR values for the self-juxtaposition for F10 vary from >35% using the V_{sh}sedsim and >30% using the V_{sh}gamma. The SGR values for the self-juxtaposition for F11 and F14 vary from <20% to >50% using the V_{sh}sedsim and >35% using the V_{sh}gamma. Most of the smaller faults in Block B (F4, F5, F6, F9, F15) show SGR values for the self-juxtaposition using the V_{sh}sedsim and the V_{sh}gamma >25%.

Based on the static geological model presented here fault F10, delimiting the Block B to the east, is the only fault that shows a juxtaposition of the Wonnerup Member against the Eneabba sandstone overlying the Yalgorup and basal Eneabba inferred top seals (Figure 14). All the other faults interpreted in the SW Hub show the Yalgorup and basal Eneabba inferred top seal forming a juxtaposition seal against the Wonnerup Member. The SGR calculation for this juxtaposition exceeds the empirical 20% threshold for faults sealing hydrocarbon (Yielding, 2002). Using the V_{sh}gamma SGR is around 45%, however using the V_{sh}sedsim SGR varies between 50% and a lowest value of 23% close to the threshold (Figure 15).

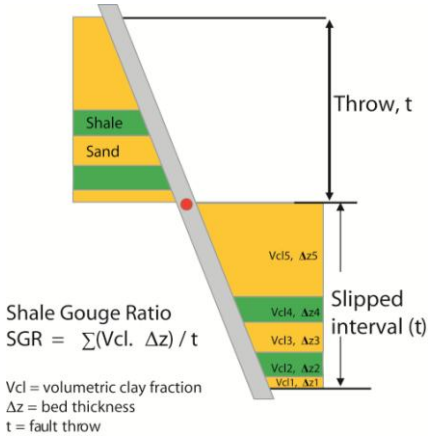

Figure 11: Schematic diagram showing definition of Shale Gouge Ratio (SGR), after Yielding et al. (1997). At any point on the fault surface, the SGR is equal to the net shale (or clay) content of the interval (t) that has slipped past that point.

Fault	Juxtaposition seal (Wonnerup –regional seal)		Self-juxtaposition (Wonnerup –Wonnerup)	
	% SGR from V_{sh}gamma	% SGR from V_{sh}sedsim	% SGR from V_{sh}gamma [max offset]	% SGR from V_{sh}sedsim [max offset]
F1	45-50	50-90 (north) 20-25 (south)	>35 [950m]	>45 (north), 30 (centre), <20 (south) [950m]
F10	45	30-85	>30 [1300m]	>35 [1300m]
F11	60-80	13-40	>35 [400m]	>50 (west), <20 (centre), >25 (east) [400m]
F14	50-80	15-30	>35 [500m]	20 [500m]

Table 2: SGR values for juxtaposition seal and Wonnerup self-juxtaposition in Block B.

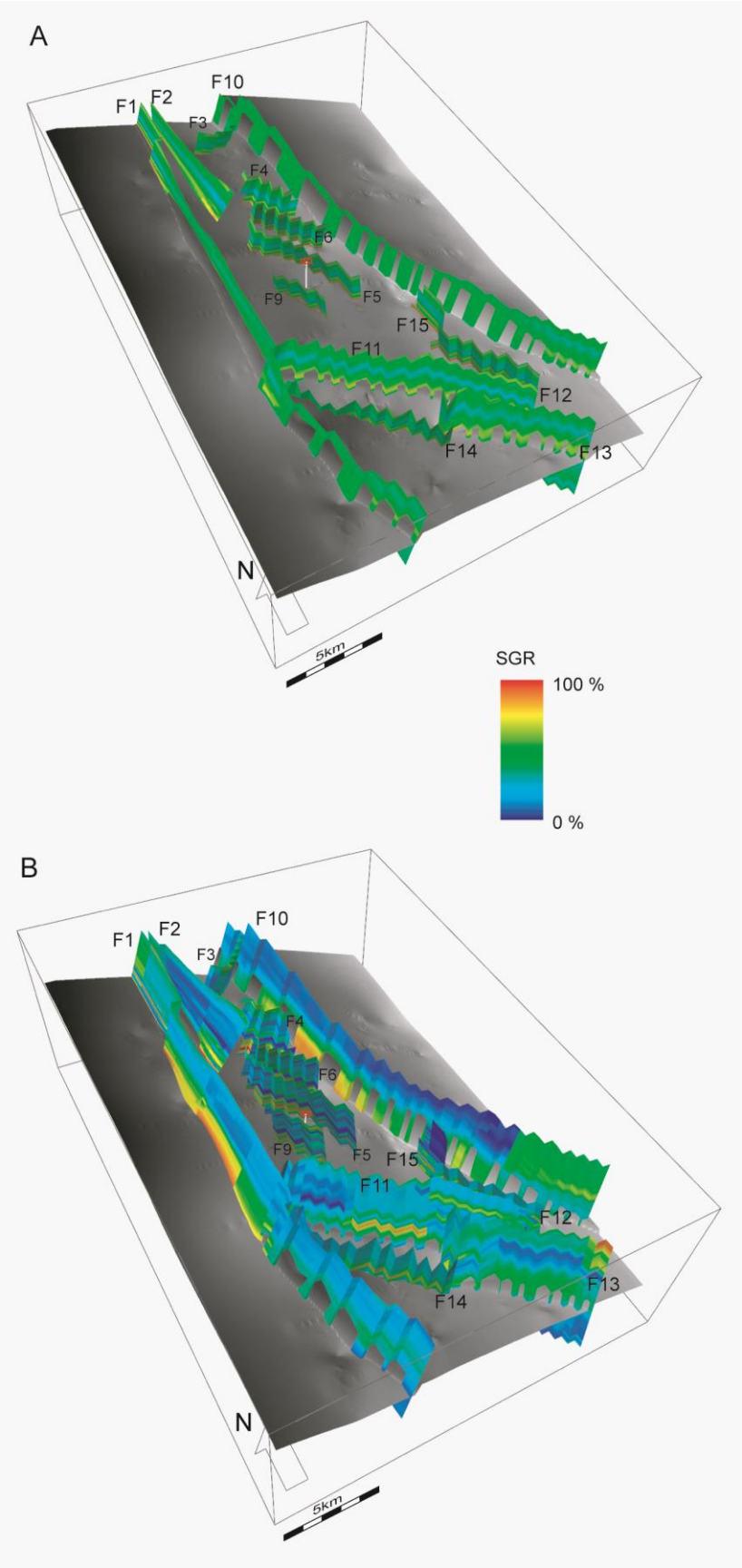

Figure 12: SGR distribution for the SW Hub. A) SGR using V_{sh}gamma. B) SGR using V_{sh}sedsim.

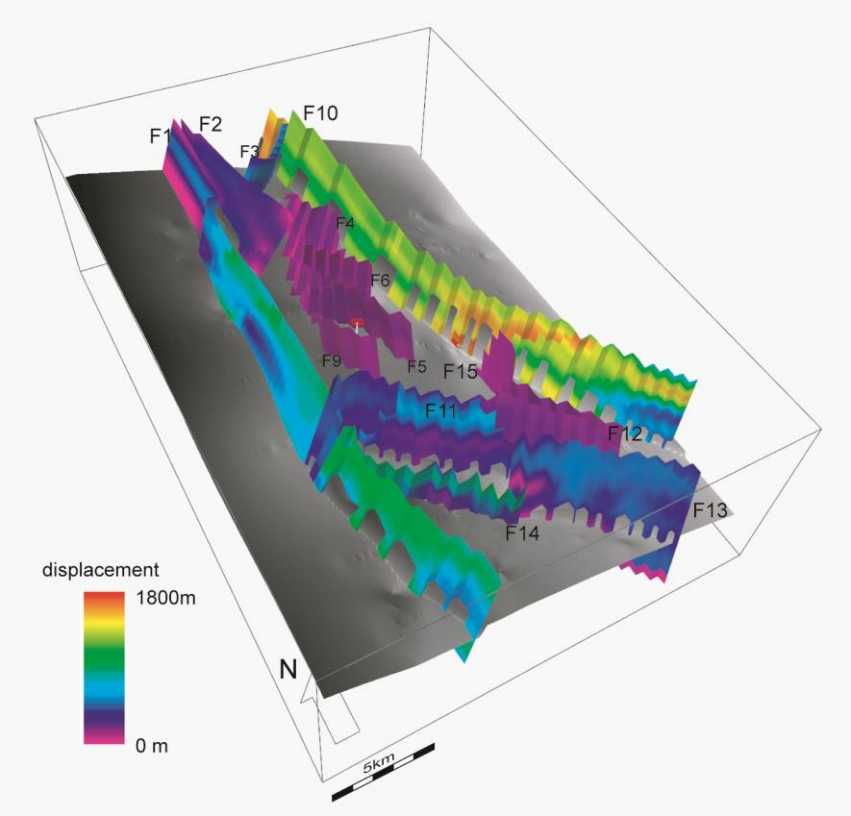

Figure 13: Displacement on faults and top Wonnerup surface.

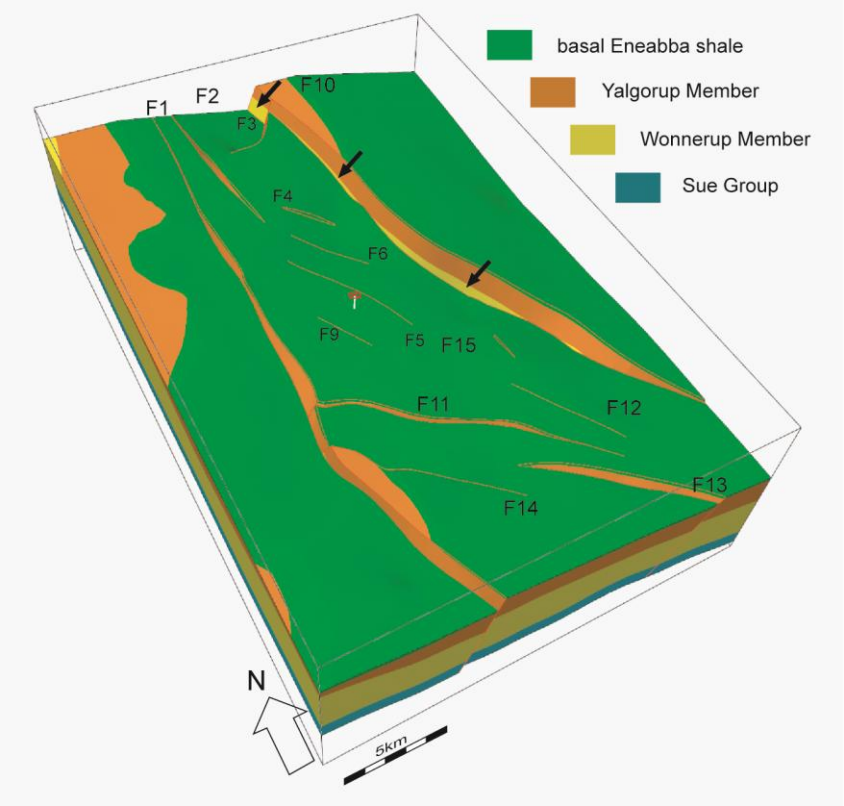

Figure 14: Juxtaposition pattern for the Wonnerup Member. The juxtaposition between the Wonnerup Member (yellow) and the Eneabba Formation (not shown, above the basal Eneabba shale in green) only occurs at fault F10 (black arrows).

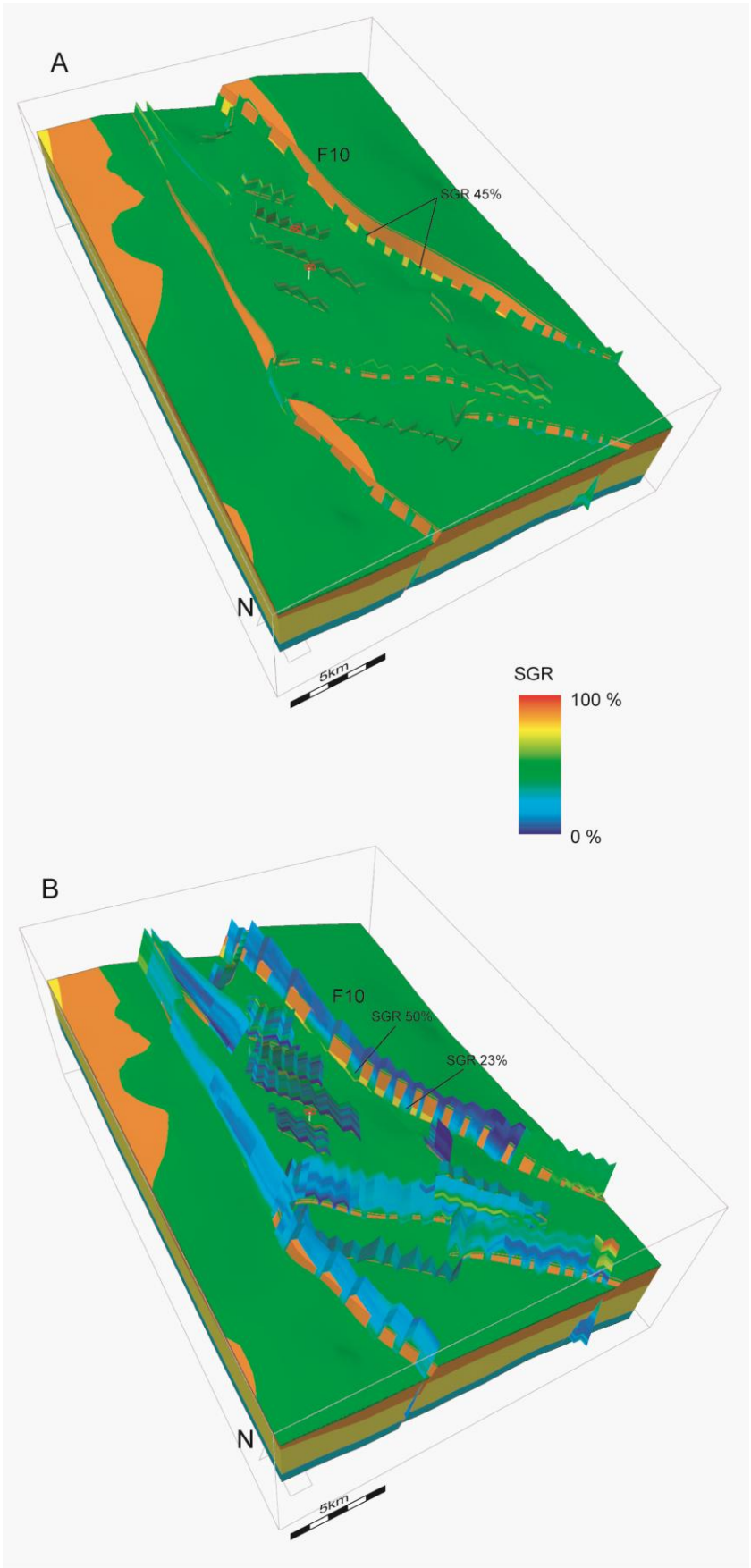

Figure 15: SGR associated with the Wonnerup-Eneabba juxtaposition. A) SGR using V_{sh}gamma. B) SGR using V_{sh}sedsim.

5.2 Geomechanical fault seal prediction

Active or critically-stressed faults intersecting the caprock are often cited as more likely to be fluid conduits whereas inactive or non-critically stressed faults are thought more likely to act as barriers (e.g. Sibson, 1987; Muir-Wood and King, 1993; Anderson et al., 1994; Barton et al., 1995; O'Brien et al., 1999; Sanderson and Zhang, 1999; Wiprut and Zoback, 2000; Zoback and Townend, 2001; Revil and Cathles, 2002; Ligtenberg, 2005; Wilkins and Naruk, 2007).

Characterising the stress state of a fault plane is a key aspect for assessing the risk of along-fault hydrocarbon leakage (Wiprut and Zoback, 2000). When plotted on a Mohr diagram (Figure 16), faults lying above the failure envelope are reactivated and likely to be conductive (Barton et al., 1995). This is supported by evidence showing that seal breach by fault reactivation represents a critical exploration risk for hydrocarbons in many petroleum provinces (Smith, 1966; Sibson, 1996; Abrams, 1996; Kaluza and Doyle, 1996; Dewhurst and Jones, 2002; Dewhurst et al., 2002, Gartrell and Lisk, 2005; Langhi et al., 2010).

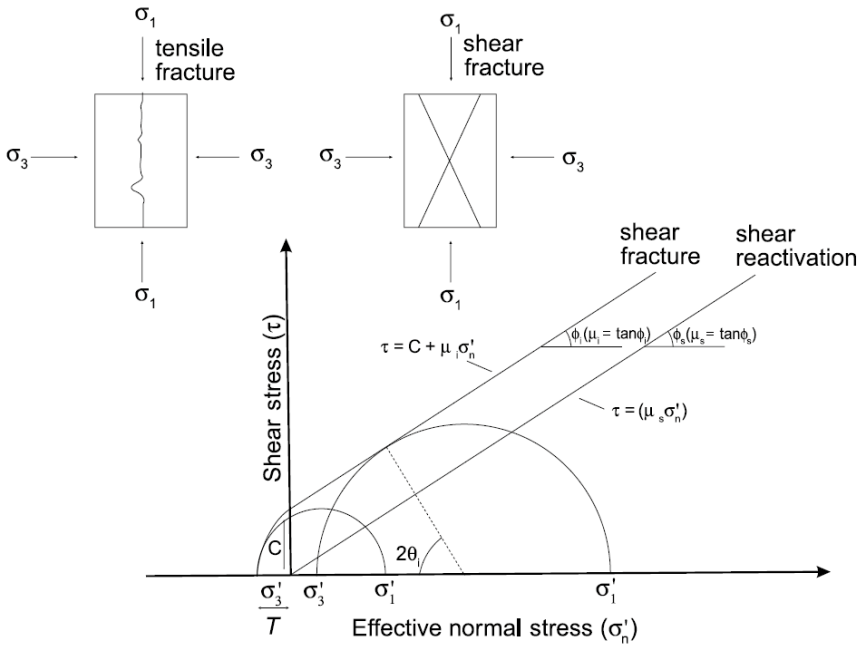

Figure 16: The effective normal (σ'n) and shear (τ) stresses leading to shear and tensile fracturing assuming a cohesionless Coulomb failure envelope (τ = μsσ'n) for shear reactivation of a pre-existing fracture and a composite Griffith (τ2 - 4T σ'n - 4T2 = 0) – Coulomb (τ = C + = μiσ'n) failure envelope for intact rock. The upper diagrams are schematic illustrations of the orientations of tensile and shear fractures in a rock sample. Shear fracturing occurs where differential stress (σ1 - σ3, the diameter of Mohr circle) is relatively large compared to the tensile or cohesive strengths and tensile fracturing at Fault Seal Risks Associated with Clay-rich Lithologies relatively lower differential stress. The symbol μs is the static friction coefficient along an existing plane of weakness; and μi is the internal coefficient of rock friction for intact rock (Mildren et al., 2005).

The SW Hub stress tensor is resolved onto the modelled faults to compute the shear and normal stresses, and the faults are colour-coded by the resultant value of slip tendency which is the ratio of resolved shear stress to resolved effective normal stress on a surface (Morris et al., 1996) and that determine the stability or failure risk of a plane of weakness (Morris et al., 1996; Lisle and Srivastava, 2004). Slip is likely to occur on a surface if resolved shear stress equals or exceeds the frictional sliding resistance.

$$T_s = \tau/\sigma_{n\,eff} \geq \mu \qquad (2)$$

where τ is the shear stress, $\sigma_{n\,eff}$ the effective normal stress (σ_n minus fluid pressure), and μ the coefficient of friction on a pre-existing fault plane. Byerlee (1978) shows that, for an effective normal stress ≥ 10 MPa, μ is within the range 0.6-1.0. Therefore a slip tendency of 0.6 corresponds to the (lowest) frictional strength of a cohesionless rock surface, and can be considered an approximate estimate of the stress state that

would induce slip and therefore cause the fault to act as a fluid conduit (Bretan et al., 2011). The slip tendency analysis is a technique that permits rapid and easy visual assessment of stress states and related potential fault activity (Moeck et al., 2009). However this represents a "relative" measurement potential of fault activity. For planes that are under an overall similar in-situ stress an increase of slip tendency correlates with an increase in potential fault activity because on a Mohr diagram the fault plane is closer to the failure envelop. However for planes that are not under an overall similar in-situ stress (e.g., due to important variations of depth between the planes) an increase of slip tendency will not always correlate with an increase in potential fault activity because on a Mohr diagram the fault plane with the lower slip tendency value might be closer to the failure envelop than the one with higher slip tendency value.

A way to overcome this limitation is to use the fracture stability attribute (Mildren et al., 2005) that represents the critical pore pressure perturbation required to induce failure on a particular fault orientation. This attribute can be computed assuming a cohesionless frictional failure (e.g., Finkbeiner et al., 2000; Wiprut and Zoback, 2000) or assuming faults with cohesive strength (Dewhurst and Jones, 2002; Jones et al., 2002). For the SW Hub the variation of depth to the top Wonnerup Member is as much as 1000 m, therefore the fracture stability is also used to quantify the possibility of reactivation-related seal breach. The pore-pressure increase might occur as a result of a new buoyant supercritical CO_2 column.

The critical column height corresponding to the pore-pressure increase P depends on the fluid densities:

$$h_{max} = P/(\rho_w - \rho_h)g \quad (3)$$

where ρ_w and ρ_h are the densities of water and buoyant fluid and g is the acceleration due to gravity.

The in-situ stress data for this study (Figure 17) comes from the integration of data from Harvey-1 (Pevzner et al., 2013). It represents a strike-slip regime (SHmax> Sv>Shmin) (Van Ruth, 2006) that transitions to a reverse regime at depth < c. 500m. For the calculation of the slip tendency and the fracture stability, the vertical stress (Sv) gradient is 0.0217 MPa/m and has been derived from the integration of density data form Harvey-1 (Pevzner et al., 2013) . The minimal horizontal stress (Shmin) is estimated using the bilateral constraint (Zoback, 2007) and the maximum horizontal stress (SHmax) is estimated from the frictional equilibrium criterion for the strike-slip fault regime (Zoback, 2007). The gradient used for the horizontal stresses (SHmax and Shmin) are set to 0.0261 MPa/m and 0.018 MPa/m respectively. This results, for the calculated stress attributes, in a stress state at 600 m below ground level characterised by Shmin=12.3 MPa, SHmax=15.2 MPa and Sv=13.0 MPa. These linear parameters give an unrealistic stress regime with SHmax<Shmin at depth shallower than 250m, therefore stress attributes should be ignored for that depth range. Based on borehole breakout analysis SHmax has orientations between 085° and 120° in Harvey-1 with an average orientation of 106° (Pevzner et al., 2013).

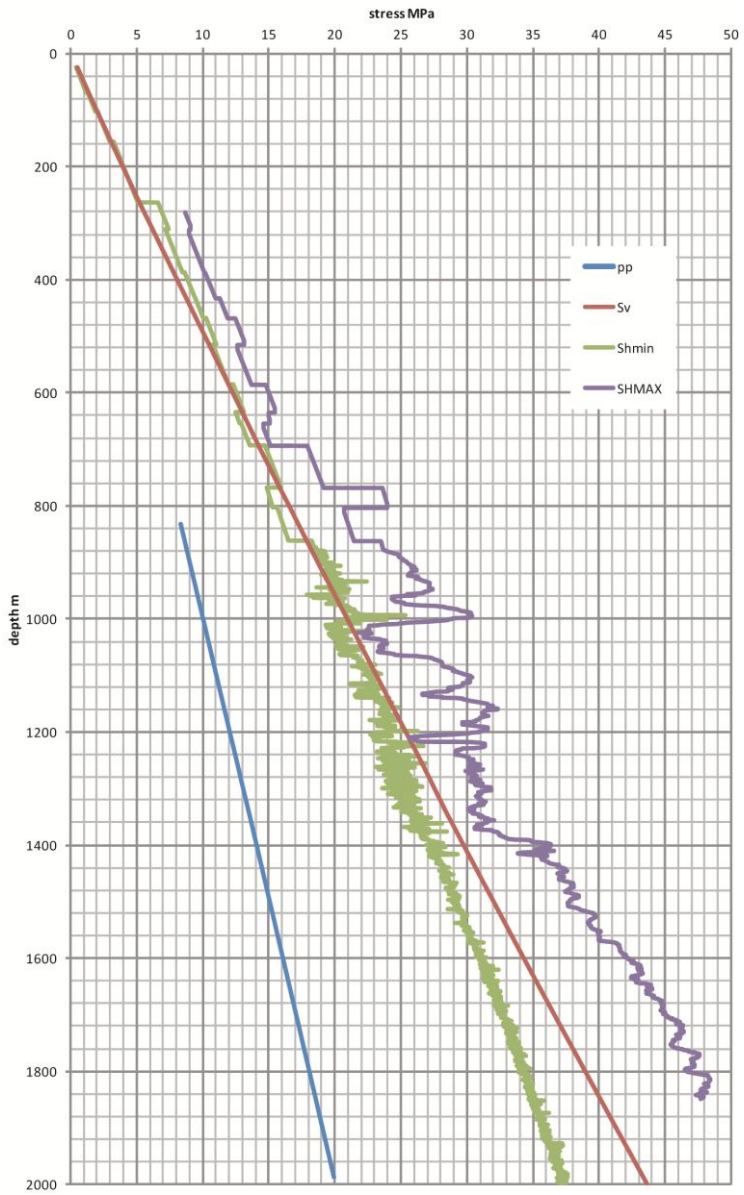

Figure 17: In-situ stress field derived from Harvey-1.

Stress state on fault planes

The slip tendency (T_S) values are minimum for faults striking parallel to SHmax and Shmin (105° and 195° respectively). T_S increases for strike orientation 50°-80° (SW-NE) and 130°-160° (SSE-NNW) (Figure 18). Using the strike-slip regime defined above, none of the faults modelled for the SW Hub are predicted close to failure. Slip tendency values at the top Wonnerup Member are lower than 0.6, typically between 0.15 and 0.3 (Figure 19). Due to a change in its strike orientation the large N-S fault F1, delimiting the western side of the Block B, shows a variation in slip tendency with a slight increase to the south of the fault (Figure 19). However, a maximum slip tendency of c. 0.2 at top reservoir level is still well below the lowest frictional strength of a cohesionless rock surface and suggests a low risk of reactivation. Faults in the Block B as well as the large fault F10 to the east are all or partly optimally oriented (i.e., NW to NNW, Figure 18). However, again, a maximum slip tendency is around 0.3 at top reservoir level.

The fracture stability (i.e., pore pressure perturbation required to force a fault into failure) has been calculated using a coefficient of internal friction of 0.5 and a cohesive strength of 3 MPa (Figure 20) and then converted to an equivalent of maximum CO_2 column height using the equation (3) and a supercritical

CO_2 density of 370kg/m^2. This shows the predicted amount of trapped CO_2 column that would be required to induce fault slip and therefore to cause up-dip fault leakage out of the Wonnerup Member (Figure 21). On most of the faults for the SW Hub, CO_2 column heights in excess of 1200 m are needed to reach failure stress (at the top Wonnerup level). The lowest column heights correlate with a shallow top reservoir; this is visible in the northern part of fault F1, F2 and F10 with c. 1200m CO_2 column height required to force planes into failure (equivalent to 8 MPa fracture stability). The NNW to NW faults present in Block B typically show a maximum of CO_2 column height around 2000m at the depth of the top reservoir (Figure 21).

The CO_2 column height can also be computed assuming cohesionless faults (cohesive strength 0). This could represent a conservative approach to evaluate reactivation potential due to increase of pore pressure. The overall column height distribution pattern is similar than with the fracture stability but CO_2 column height values decrease between 5% and 30% depending the depth with an average decrease of around 20%.

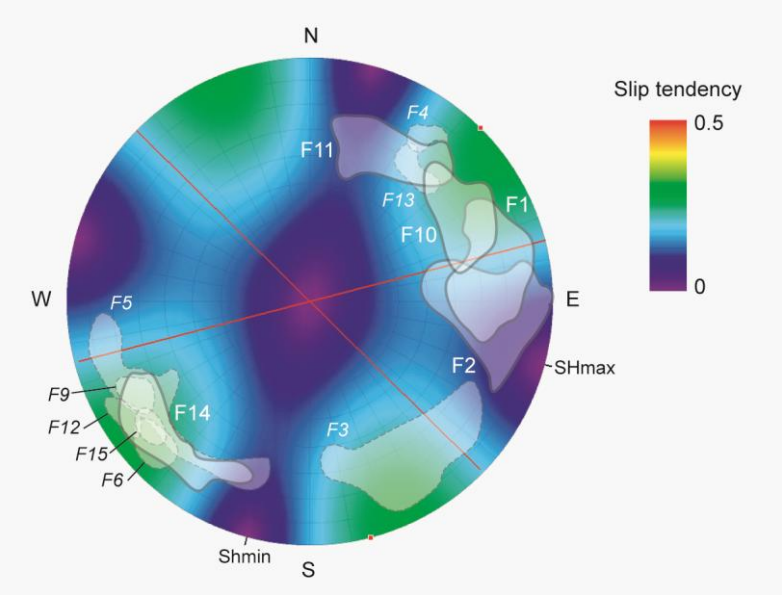

Figure 18: Slip tendency stereonet at 1500 m. The orientations of the faults are used in the stress calculation. The poles of the faults are plotted on the stereonet. The subsidiary fault planes are labelled in italic.

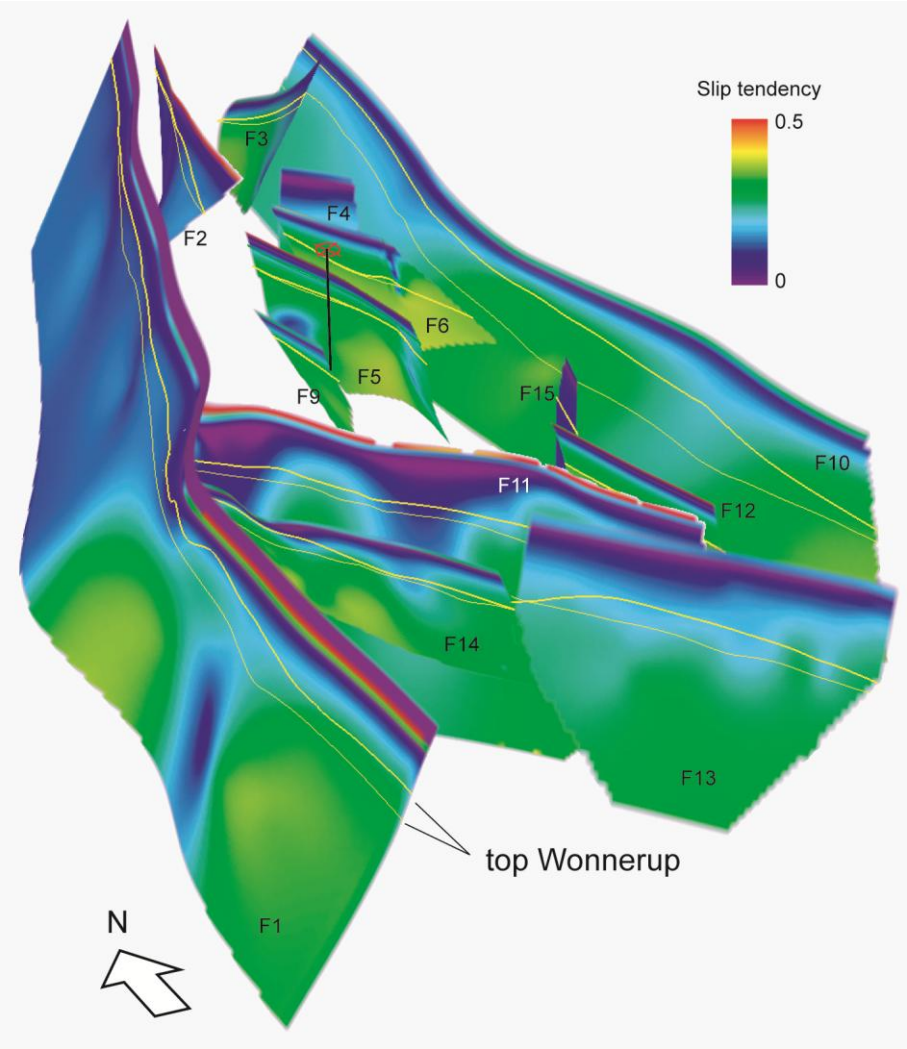

Figure 19: Slip tendency distribution. The cutoff lines for the top Wonnerup are in yellow (footwall=bold, hanging-wall=regular).

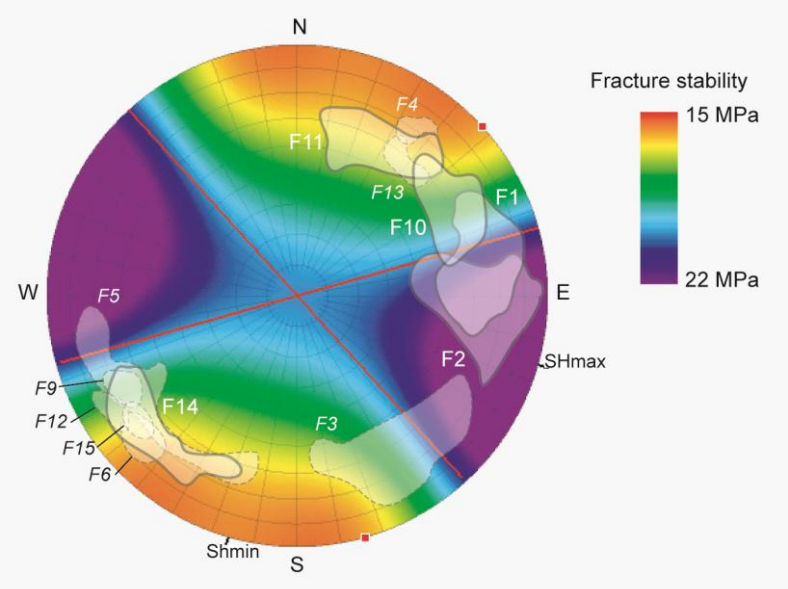

Figure 20: Fracture tendency stereonet at 1500 m. The orientations of the faults are used in the stress calculation. The poles of the faults are plotted on the stereonet. The subsidiary fault planes are labelled in italic.

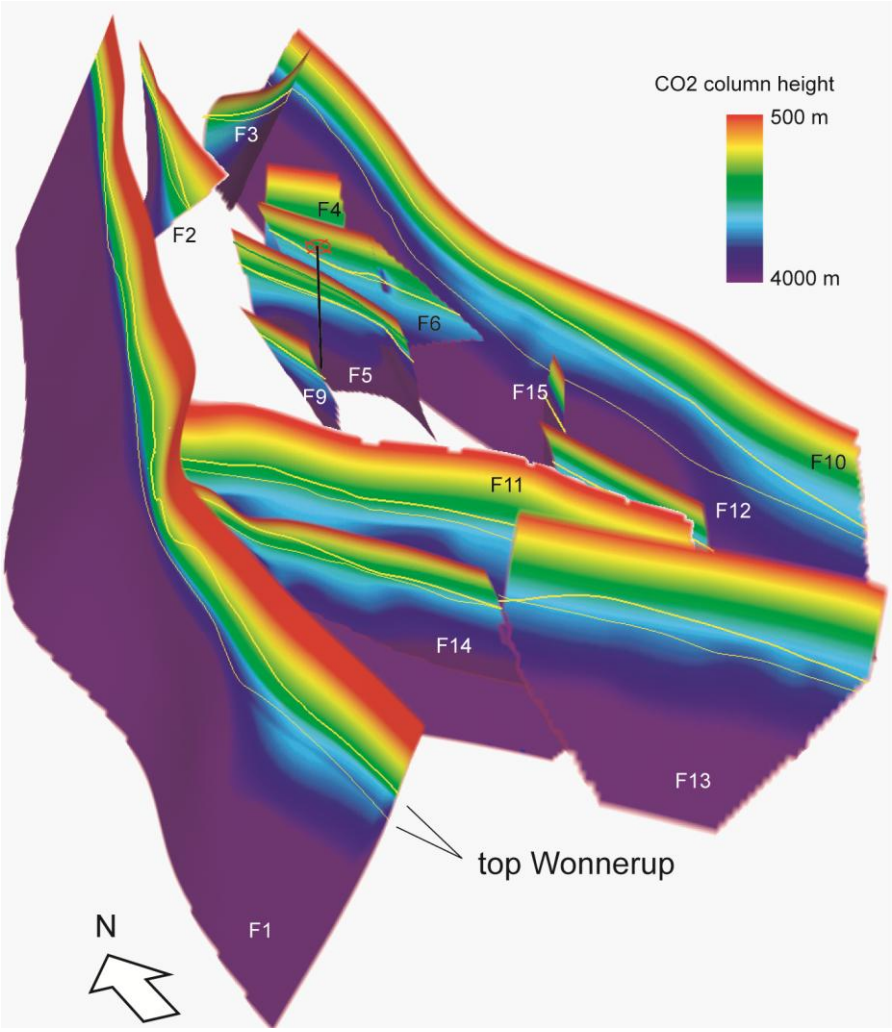

Figure 21: Equivalent of maximum CO_2 column height calculated from fracture stability. The cutoff lines for the top Wonnerup are in yellow (footwall=bold, hanging-wall=regular).

5.3 Implications of fault seal assessment for CO_2 storage

The containment potential for injected CO_2 in the SW Hub can be affected by four migration scenarios controlled by fault seal:

1. lateral migration of CO_2 between reservoir compartments,
2. lateral migration of CO_2 between reservoir and thief zone(s) in regional seals,
3. lateral migration of CO_2 between reservoir and overburden and
4. along fault migration of CO_2 between reservoir and overburden

The likelihood of lateral migration is assessed using SGR that is a function of the phyllosilicate content in the surrounding host rock and the displacement on the fault (Yielding et al., 1997; Freeman et al., 1998). Both these parameters present uncertainties due to (1) the low density of seismic reflection data limiting the definition of fault displacement patterns and (2) the lack of data and calibration for lithological facies distribution (i.e., V_{sh}). Therefore the calculation and interpretation of SGR represent only a first-order assessment of the across-fault migration potential for the SW Hub. The use of two V_{sh} models (i.e., V_{sh}gamma and V_{sh}sedsim) allows for definition and assessment of two different scenarios. In overall the SGR values derived from V_{sh}sedsim present the more extreme variations with the lowest (i.e., 13%) and the highest (90%) prediction (Figure 12b), while the SGR values derived from the inversion of gamma-ray log in

Harvey-1 shows a more restricted range with values generally around 40% (Figure 12a). The discussion below includes both SGR calculations but emphasis is put on the lowest values and therefore represent a rather conservative (i.e., pessimistic) interpretation.

The likelihood of lateral migration across faults within the Wonnerup Member (i.e., self-juxtaposition) is high to average at several locations using SGR derived from V_{sh}sedsim (southern F1, central F11, F14). This suggests that CO_2 containment might be at risk in the southern part of Block B with potential of migration to the west into Block C if the CO_2 column exceeds the local offset (c. 300m, Figure 22). The potential of lateral migration across faults within the Wonnerup Member in the Block B is mostly average to low with SGR usually above 25% except for the central part of F11 and the eastern part of F14 (Figure 22).

The likelihood of lateral migration across faults between the upthrown Wonnerup Member and any interbedded sandstone in the Yalgorup Member can be locally high. Using V_{sh}sedsim, SGR values below 20% occurs on F11 (13% in the western and central parts of the fault plane), on F14 (15% in the eastern part of the fault plane) and at the southern end of F1 (Figure 22). This again suggests that CO_2 containment might be at risk in the southern part of Block B with potential of migration to the west into Block C (sandstone layers in the downthrown Yalgorup Member).

Lateral migration across faults between the upthrown Wonnerup Member and the overburden Eneabba Formation is only possible at fault F10. However SGR values derived from both V_{sh}sedsim and V_{sh}gamma are above the 20% threshold for faults sealing hydrocarbon (Yielding, 2002). Using equation (1) with a supercritical CO_2 density of 370kg/m^2, the possible CO_2 column heights that can be supported by fault F10 before the buoyancy pressure exceeds the capillary entry pressure are:

- c. 700 m, with V_{sh}gamma and SGR 45%,
- c. 1100 m, with V_{sh}sedsim and SGR 50%, and
- c. 110 m, with V_{sh}sedsim and SGR 23%.

The lowest SGR and potential CO_2 column height is found toward the centre of F10 (Figure 22). It is to be noted that although membrane seal capacity is reasonably constrained over production time scales (10's of years), the capacity over the geological time scales (million years and above) is still questioned by some researchers (T. Murray, personal comm., 2012).

The likelihood of vertical migration along faults between the Wonnerup Member and the overburden is assessed using the slip tendency, fracture stability and slip stability attributes that are functions of the shear and normal stresses on the fault plane and the distance to the failure envelop (i.e., the pore pressure perturbation required to induce failure). Both these parameters present uncertainties due to (1) the low density of seismic reflection data limiting the resolution of fault geometry, (2) the lack of rock physics data limiting the definition of failure envelops and (3) limitation of data for the calibration of the in-situ stress field. Therefore the calculation and interpretation of the geomechanical attributes represent a first-order assessment of the along-fault migration potential for the SW Hub.

The main and subsidiary faults in Block B are optimally oriented for failure (NNW and NW, Figure 23). However, the high stress state at the depth of the Wonnerup Member results in a low slip tendency below the empirical typical threshold of 0.6 suggesting a low risk of fault failure under the present-day stress (Figure 23).

The maximum CO_2 column height theoretically supported by a fault plane and calculated from the fracture and slip stability (equation (3)) is marginally orientation-dependant with slightly lower values for strike orientations between 50° and 160° (SE-NW to ENE-WSW) especially for fault with dip > 60°. However the depth has the most impact as an increasing depth moves the Mohr Circle away from the failure envelop and therefore increases the potential CO_2 column height. Based on the pore pressure perturbation required to induce failure on a particular fault orientation (i.e. vertical distance between the fault and the failure envelop on a Mohr diagram), the theoretical smallest CO_2 column heights required to reach failure stress are located to the north of Blocks A and B along faults F1, F2 and F10 and represent 1200m or 1000m when assuming a cohesive and cohesionless fault respectively (Figure 23). However, this smallest CO_2 column heights corresponds to fracture stability and slip stability values <10MPa and empirical data from Mildren

et al. (2005) in the Timor Sea suggest that a pore pressure perturbation smaller than 10 MPa is likely to result in the initiation of hydrocarbon leakage over geological times (Figure 23). With the values for density and viscosity for supercritical CO_2 being similar to those of oil and gas we assume that the observation made by Mildren et al. (2005) for oil and gas field can be applied to CO_2 injection sites.

First order geomechanical fault seal assessment suggests that the faults in Block B are unlikely to fail and reactivate under the present-day stress field. However, due to the depth of the top Wonnerup, the faults in the northern Block B are likely to require the relative lowest pore pressure increase of be force into failure.

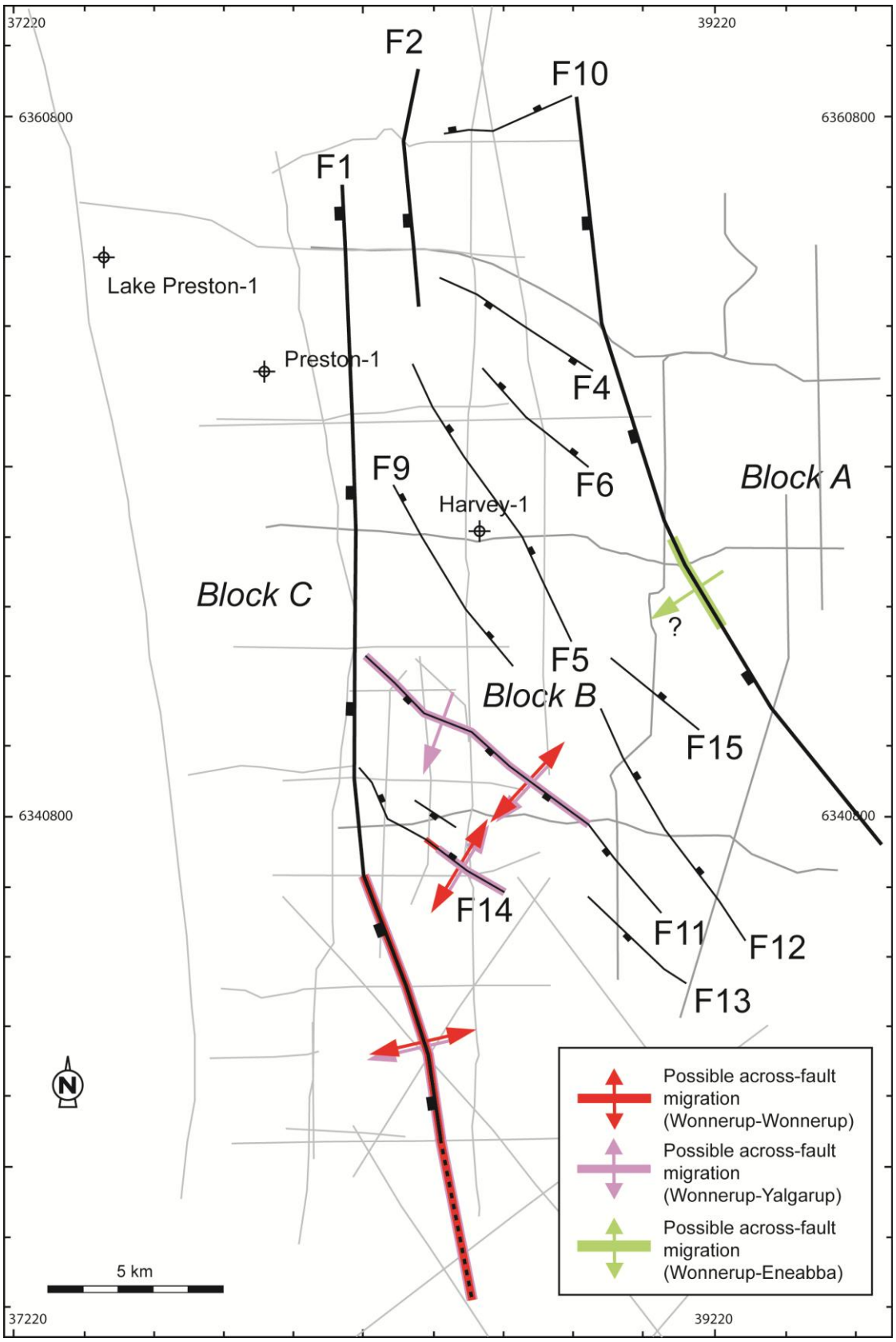

Figure 22: Summary of across-fault CO_2 migration potential for the SW Hub. CO_2 containment might be problematic in the southern part of Block B with potential of migration to the west into Block C if the CO_2 column exceeds the local offset (Wonnerup-Wonnerup migration and in thief zones in the Yalgorup Member).

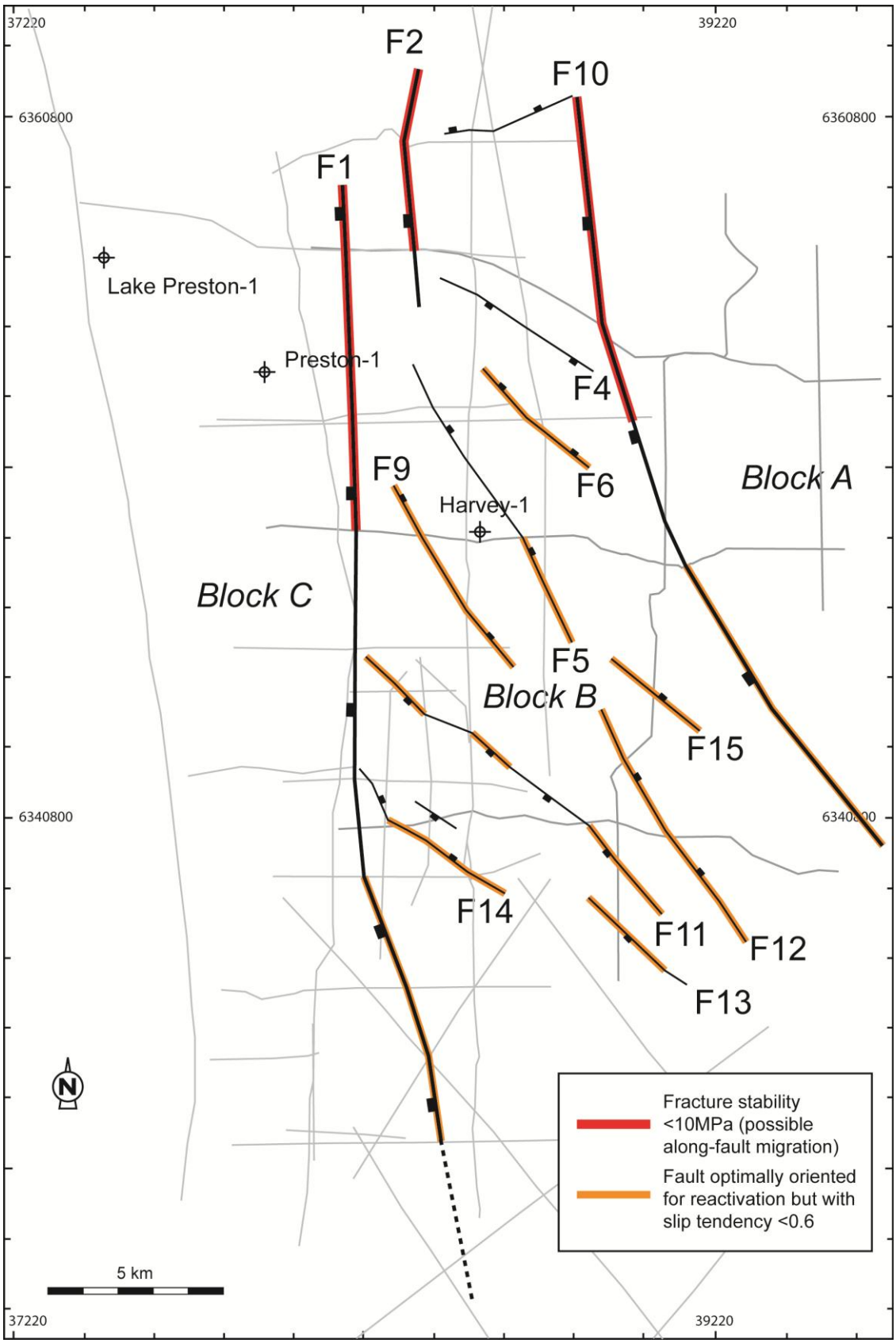

Figure 23: Summary of along-fault CO_2 migration potential for the SW Hub. The northern part of Block B is associated with the smallest CO_2 column heights required to reach failure stress.

6 Fracture prediction

It is well established that small brittle faults are not reliably imaged by seismic reflection methods when their offset is less than the seismic resolution (i.e., about 20 m in most datasets, Dee et al., 2007). In recent years geomechanical approaches have been used to predict the likely distribution of subsurface strain, and then to transform it to stresses to predict the intensity and nature of brittle deformation (Bourne and Willemse 2001; Bourne et al. 2001; Maerten et al. 2002; Dee et al., 2007). We adopt here an approach detailed by Dee et al. (2007) and use a boundary element method (BEM), in which faults are represented as dislocations embedded in an isotropic elastic medium (Crouch and Starfield 1983). We assume for the SW Hub that a dominant control on small-scale faulting is the strain perturbation around larger faults. Variations of rock properties that occur in layered sedimentary sequences are not considered in the strain modelling, only in the fracture criterion. Despite this limitation Dee et al. (2007) demonstrate that the method is useful in providing a process-driven prediction of small-scale faults and fractures.

The workflow used follows that described by Maerten et al. (2002) and Dee et al. (2007). The fault slip pattern mapped on seismic reflection data is the primary input data; the algorithms of Okada (1992) are then used to compute the displacement vector and fault-related strain tensor at any observation points in the surrounding rock volume. As the fault-related strains represent a local perturbation superimposed on the regional far field strain, this latter has to be defined and added at every observation point. The strain tensors are then used to calculate stress tensors and the effective overburden stress is added. The predicted rock fracturing resulting from the total stress is then computed by comparing the state of stress to a standard Mohr–Coulomb failure envelope, defined by appropriate coefficient of internal friction μ and cohesive strength C. to determine the mode of failure the $\Delta\chi$ method from Willsemse (2001) is used. The maximum Coulomb shear stress (MCSS, Jaeger and Cook 1979) is used as a proxy for fracture intensity (Maerten et al., 2002).

For the SW Hub, the elastic dislocation method (ED) is used to attempt to define a first order prediction of the small-scale subsidiary faults and fractures for the Block B within in the upper part of the Wonnerup Member and the Yalgorup Member representing the potential regional top seal (Figure 2). These two models use (1) the same observation grid to calculate the initial displacement, (2) the same depth correction take into account real depth at the time of faulting, (3) the same regional strain to be superimposed to the ED strains and (4) two sets of rock properties Wonnerup Member and the Yalgorup top seal. The models parameters are as follows:

1. The observation grid is set to represent the interface between the Wonnerup and the Yalgorup Members. Therefore the modelled deformation can be used for both ED models. The grid has regular line spacing (500 m) with 35 columns and 56 rows oriented N-S and E-W, respectively. The resulting grid is 28 x 17.5 km (Figure 24A).
2. The bulk of the displacement on the large faults pre-dates the Neocomian Unconformity and likely occurred during the Early Cretaceous. Based on stratigraphic correlation throughout the South Perth Basin (Crostella and Backhouse, 2000) and vitrinite reflectance data from the nearby Lake Preston-1 (Iasky, 1993), we assume that at the time of faulting, 1200 m of additional Late Jurassic sediments (Eneabba and Yarragadee Formations) were present. Therefore the depth is adjusted accordingly before generating the ED model in order to obtain the likely depth of the fault planes during slip.
3. A regional strain is estimated through the measurement of the cumulative slip across structures in the SW Hub. The maximum horizontal strain has an azimuth of N263 and an estimated magnitude of 3% (extension). The minimum horizontal strain has an estimated magnitude of 1.3% (extension). Assuming a preservation of volume the calculated vertical strain is 4.2% (shortening). This estimate

represents the fault-related strain over a limited distance represented by the framework model and may underestimate the total fault related strain on the SW Hub and may not be representative of the South Perth Basin as a whole.

4. For the Wonnerup Member, static rock properties were estimated from geomechanical analysis of four cores from Harvey-1. For the Yalgorup Member, static rock properties (Poisson's Ratio and Young's Modulus) were initially estimated from velocity logs from Harvey-1 and calibrated with data from the Wonnerup Member. The values used for the ED models are shown in Table 3.

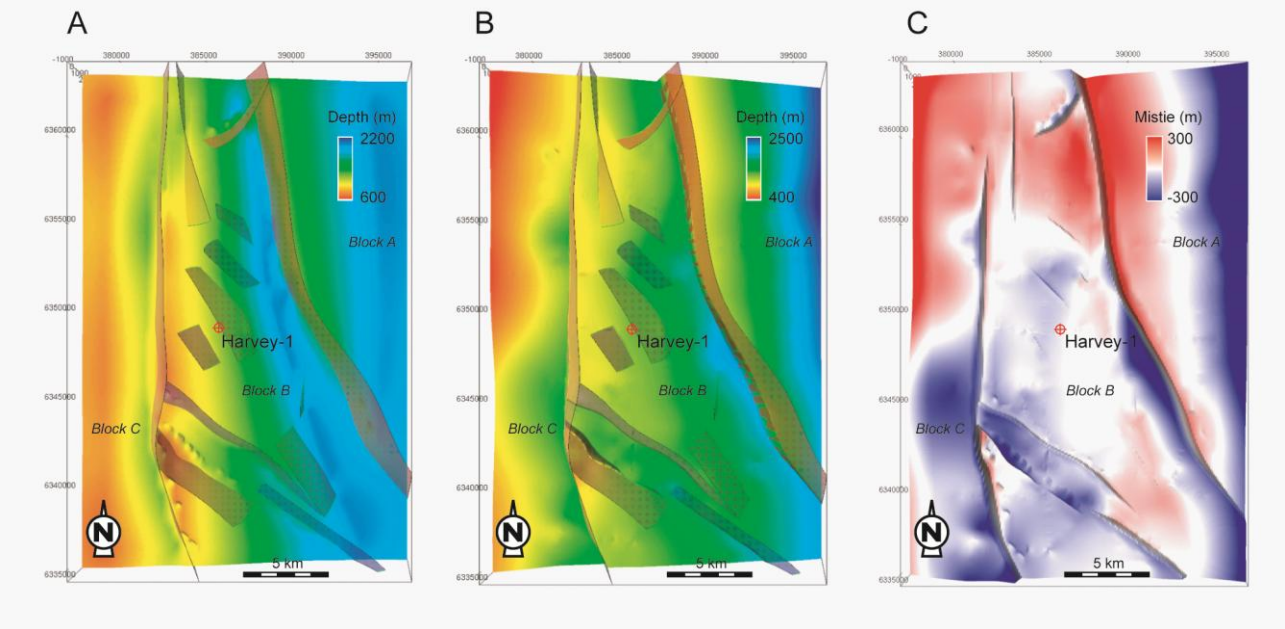

Figure 24: Deformation model. A) Deformed observation grid. B) Mapped top Wonnerup surface (Wonnerup-Yalgorup interface representing the observation grid). C) Difference between the deformed and mapped surfaces.

STRATIGRAPHIC UNIT	POISSON'S RATIO	YOUNG'S MODULUS (MPa)	DENSITY (KG/M3)	COHESIVE STRENGHT (MPa)	COEF OF INTERNAL FRICTION
Wonnerup Mbr	0.2	19250	2200	13.7	0.58
Yalgorup Mbr	0.33	8500	2000	11	0.38

Table 3: Static rock properties for the Wonnerup and Yalgorup Members.

Initially the validity of the modelled deformation is assessed by comparing the deformed observation grid with the actual mapped horizon surface. Figure 24 shows a reasonable match between them in term of the general amplitude of the deformation. Although the predicted offset at the faults is correct, as imposed by the slip distribution on the faults used as a boundary condition, misfit occurs in Blocks A and C, at the edges of the model, and to the north of Block A most likely due to the rotation of larger field bounding fault (e.g., Darling Fault to the east). However as the main focus of the present study is on Block B where Harvey-1 has been drilled, we assume that the model provides a satisfactory qualitative match to the overall form of the structure and therefore the details of predicted faulting can be considered.

The mode and orientation of predicted faulting is displayed in Figure 25. Within Block B, the imposed regional strain (extensional) produces dominantly high angle normal faulting (> 40°) within the Wonnerup and Yalgorup Members (shear failure shown in red). Overall, the orientation of the shear failure for the

Wonnerup and Yalgorup Members within Block B is similar, with only local variations, and is consistent with observations of subsidiary faults within Block B. In the close vicinity of the large fault F10 (hanging wall) there is a more complicated pattern that also involves localised reverse and strike-slip shear planes and tensile failure planes in both the Wonnerup and Yalgorup Members (Figure 25). The effect of the local perturbation of the stress field is likely to induce these types of failures in association with the dominant shear failure; however the methodology used here is also known to produce unstable result very close to the main deformation surfaces. Although a 150m blanking zone was used in the modelling around the main faults, the non shear failure observed in Block B near the fault F10 could represent numerically unstable values. These local reverse failures predicted within the Wonnerup and the Yalgorup Members in the central part of Block B and in the vicinity of fault F10 (hanging wall) also coincides with a zone of misfit between the deformed grid and the mapped horizon. The same situation is present on Block A where sinistral strike-slip failure predicted within the Yalgorup Member coincides with a zone of misfit between the deformed grid and the mapped horizon (Figure 24 and 25B).

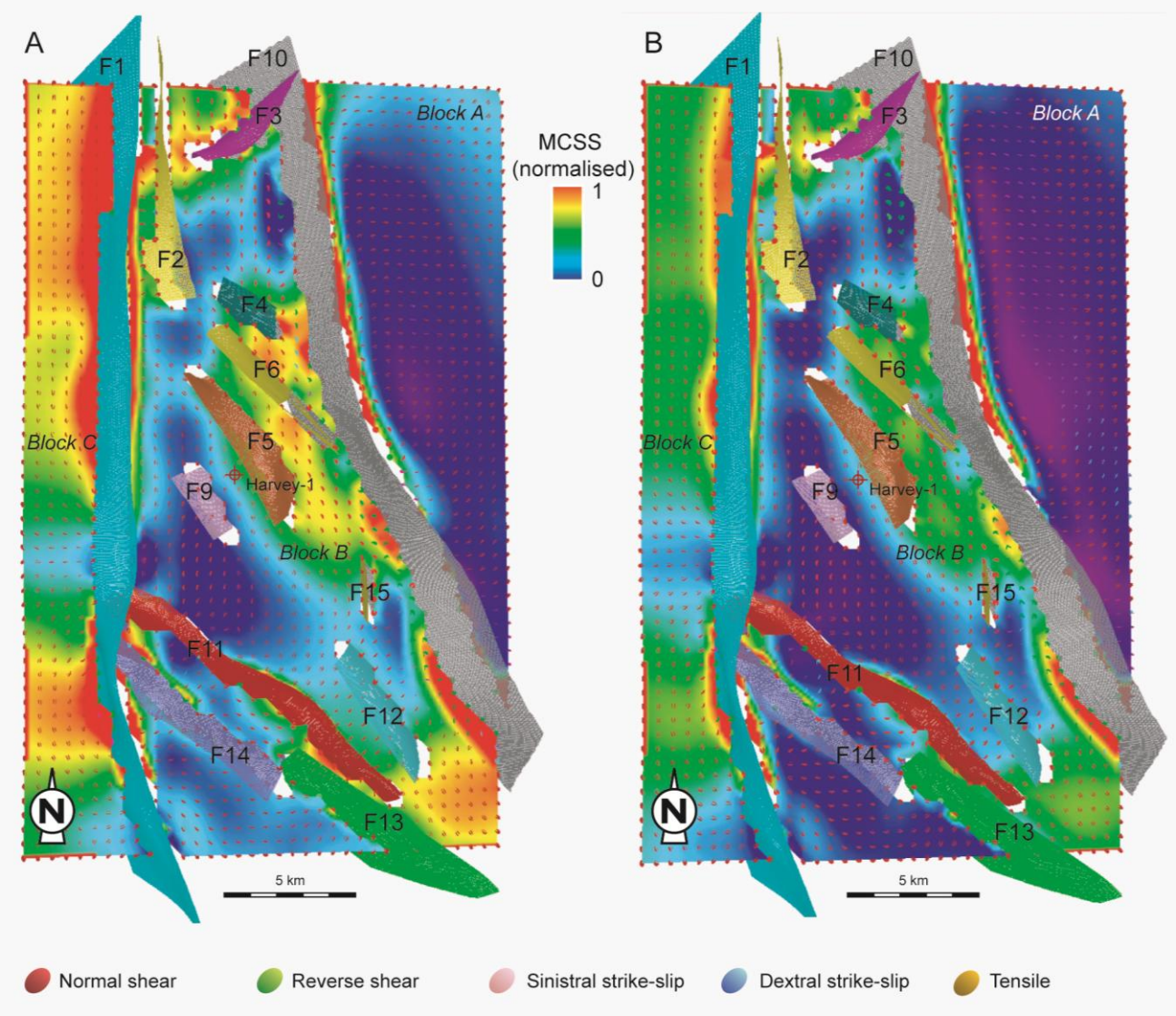

Figure 25: Modelled fractures, mode of failure and density represented by the normalised MCSS. A) Upper Wonnerup Member. B) Lower Yalgorup Member.

Predictions of fault orientation derived from the ED model are compared with actual interpreted small faults within Block B (Figure 26). The azimuth of the σ_2 orientation in map view corresponds approximately to the predicted orientation of normal-fault strike in this model (Dee et al., 2007). There is an overall correspondence between the predicted and the observed fault orientation suggesting that the model achieved a reasonable match. Precise correspondence of observed and predicted fault orientations is

seldom achieved, with areas of good correspondence (e.g., near F3, F5, F11, F14 and F15 in Figure 26) and areas of poor correspondence (e.g., near F4, F6 and F12 in Figure 26). The observed discrepancy can result from missing faults not initially interpreted, as well as the fault displacement pattern being locally inaccurate due to the low density of seismic lines. This will affect the definition of the strain tensor in the surrounding rock volume and thence the fracture prediction. This observed discrepancy could also highlight inaccurate correlations between fault sticks interpreted on 2D lines and could be used to constrain subsidiary fault orientation within Block B. Over a large part of Block B the predicted fault strikes are parallel to the main fault trends with predicted fault orientation varying from N-S to NNW-SSE. Due to local stress perturbation, SW-NE features are also predicted within the Wonnerup and the Yalgorup Members in Block B (Figure 26).

Figures 25 and 26 show the computed normalised maximum Coulomb shear stress (MCSS) for the SW Hub for both the Wonnerup and the Yalgorup Members. Warmer colours indicated where, over many seismic cycles, the shear failure envelope has been exceeded repeatedly by the highest shear stresses (Dee et al., 2007) and is therefore related to higher fracture intensity potential (Maerten et al., 2002). The qualitative distribution of MCSS is similar within the Wonnerup and the Yalgorup Members (Figures 25 and 26). The main subsidiary faults mapped within Block B (i.e., east of Harvey-1) are aligned through the maxima in the MCSS distribution even though the mapping of these faults might be equivocal. The south of Block B where it is at its widest (near fault F11), displays low MCSS. In this area no faults have been mapped on the seismic reflection data (Figures 25 and 26).

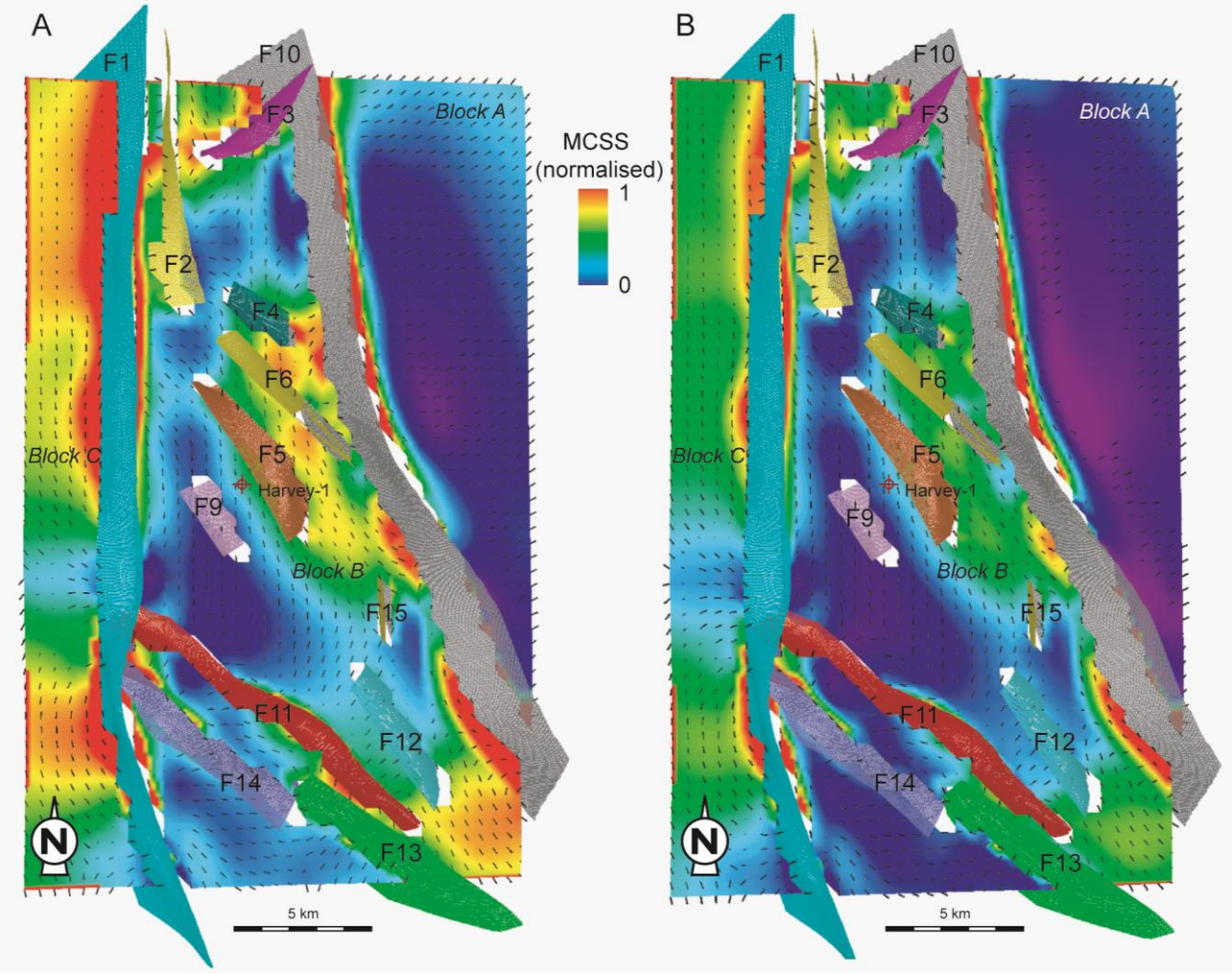

Figure 26: Modelled fractures, orientation. The azimuth of the σ2 orientation corresponds approximately to the predicted orientation of normal-fault strikes. A) Upper Wonnerup Member. B) Lower Yalgorup Member.

The predicted normal shear planes that represent most of the small-scale deformations in Block B, are likely to increase, to various degrees, the structural permeability at the time of tectonic activity (i.e., Early Cretaceous). However their impact on the CO_2 containment potential of the SW Hub has to be assessed using present-day boundary conditions (e.g., in-situ stress data, Figure 17). Figures 27 and 28 show the normal shear fracture networks colour coded with the magnitude of slip tendency and fracture stability (as in the geomechanical prediction) and the MCSS for the Wonnerup and Yalgorup interface.

The slip tendency values for the Wonnerup and the Yalgorup Members are lower than 0.6 in Block B. Fractures with orientations 50°-80° (SW-NE) and 130°-160° (SSE-NNW) and dip > 50° show the higher slip tendency (Figures 27A and 28A). A NW oriented zone of shear fractures predicted in the centre of Block B (near Harvey-1) shows higher average slip tendency values (0.17 to 0.28) for both the Wonnerup and Yalgorup Members (Figures 27A, 28A and 29). To the east of Block B, in the hanging wall compartment of F10, predicted shear fractures with dip >75° and NW orientations show highest slip tendency values up to 0.3 for the Wonnerup and the Yalgorup Members (Figure 29). The northern part of Block B, between faults F2 and F10, is subject to stress tensors rotation and shows slip tendency values for predicted shear fractures up to 0.25 especially in the Wonnerup Member (Figures 27A).

The minimum fracture stability values (<10 MPa), for the small scale fault in the Wonnerup and the Yalgorup Members, are found to the west of Block B in the footwall of the large fault F1 where the depth of the Wonnerup – Yalgorup interface is <1000 m (Figure 27B and 28B).

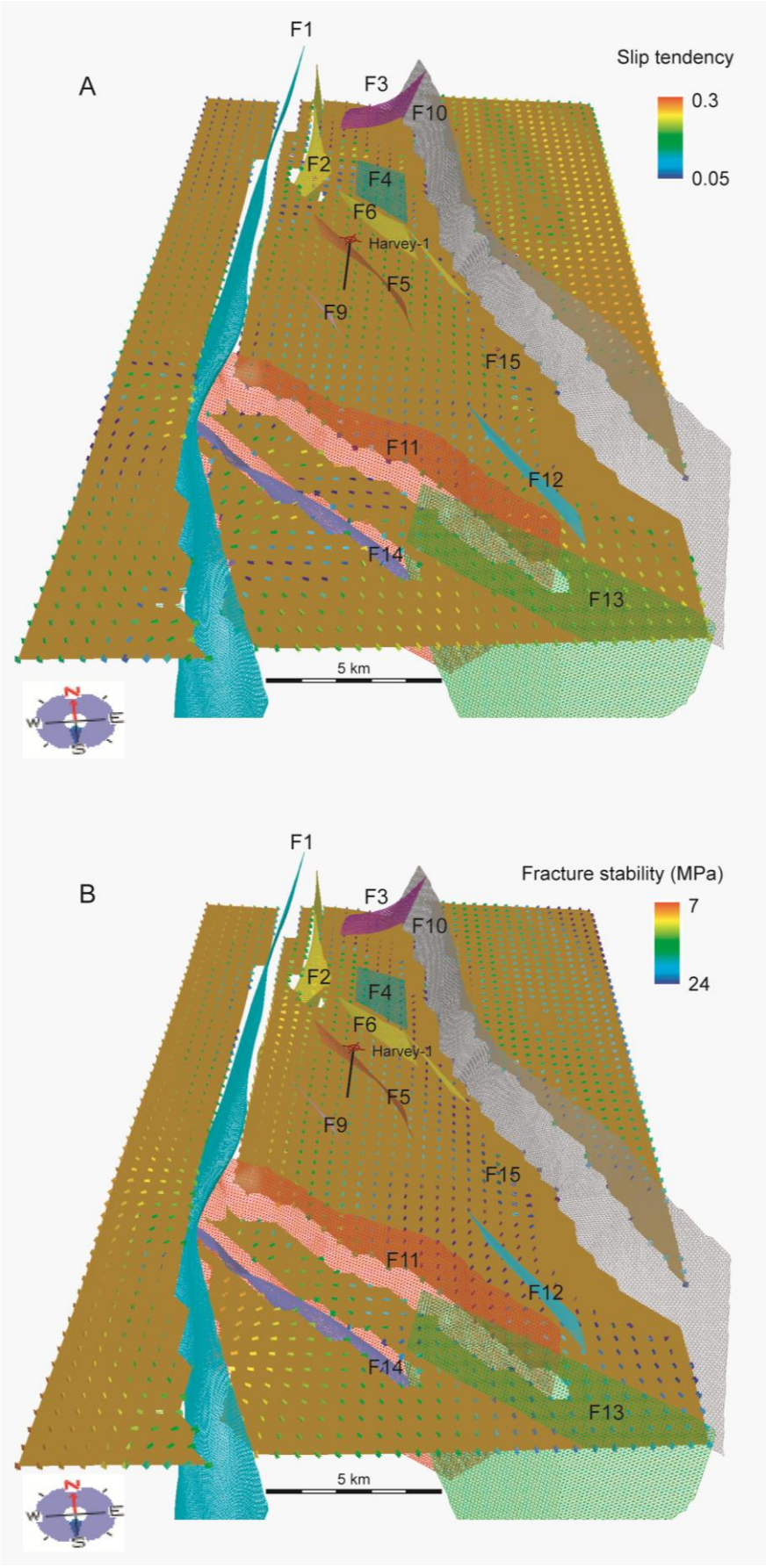

Figure 27: Geomechanics for normal shear fracture networks for the Upper Wonnerup Member. A) Slip tendency. B) Fracture stability.

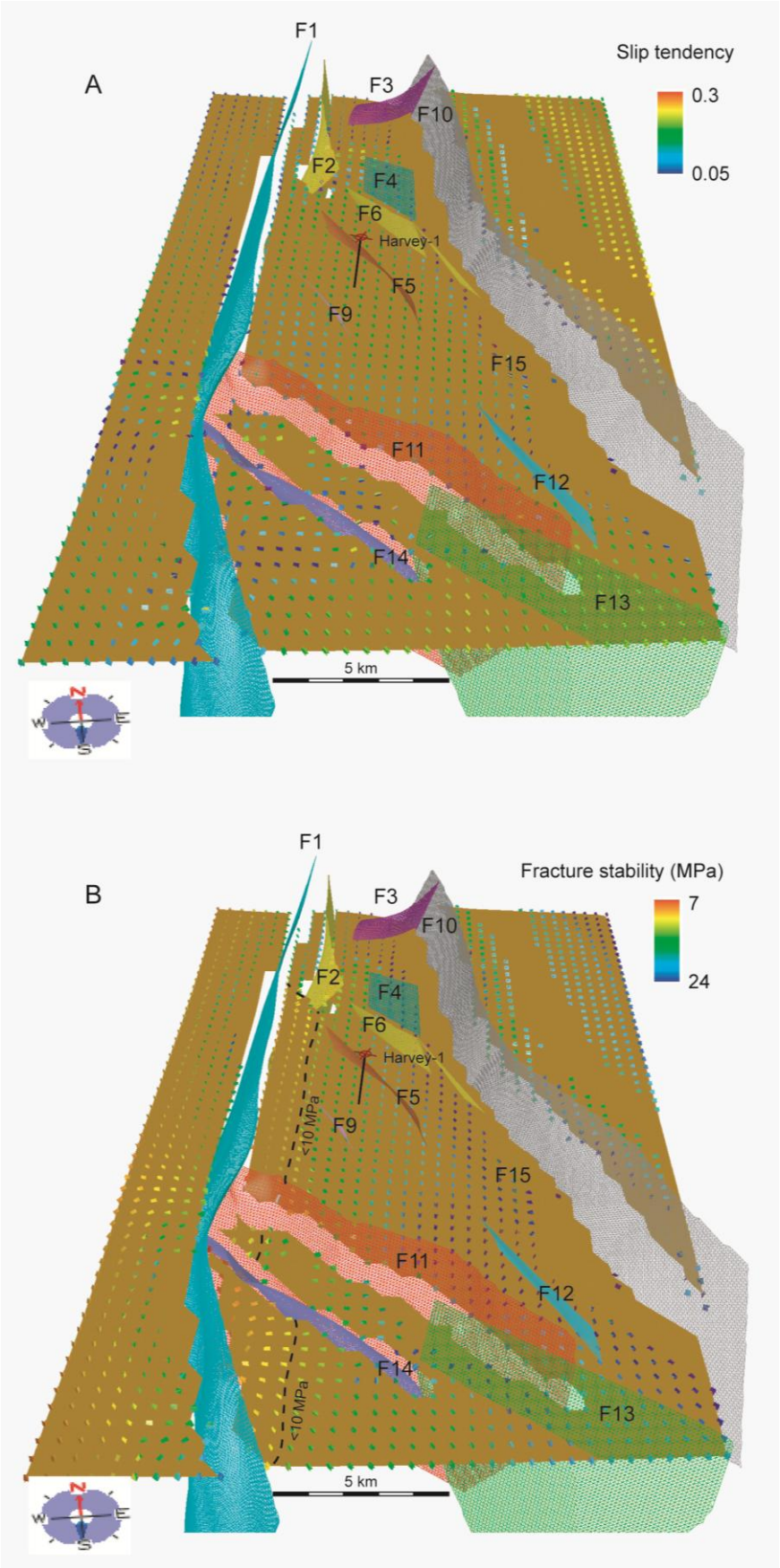

Figure 28: Geomechanics for normal shear fracture networks for the Lower Yalgorup Member. A) Slip tendency. B) Fracture stability.

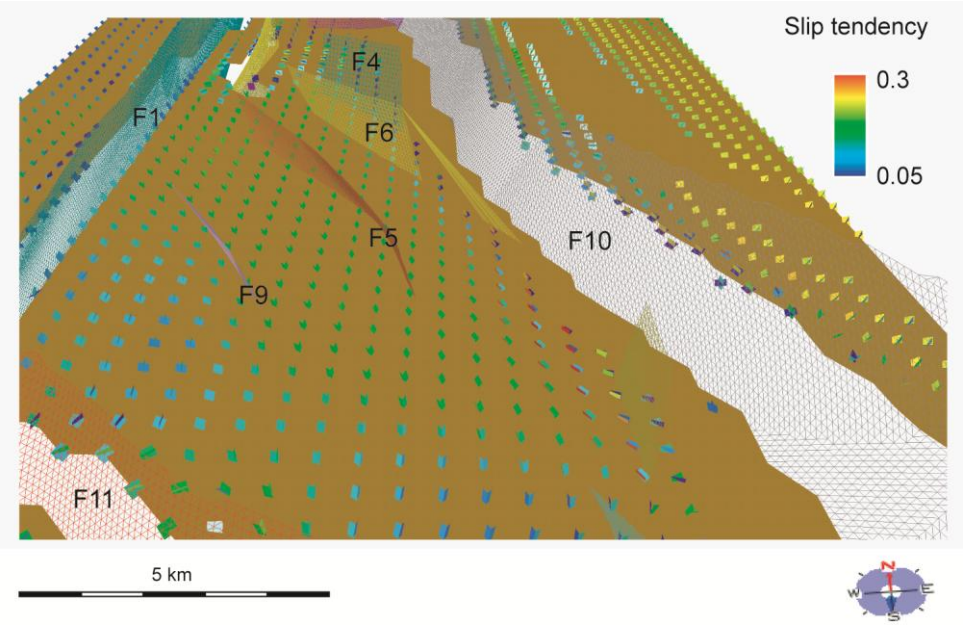

Figure 29: Geomechanics for normal shear fracture networks colour coded with the magnitude of slip tendency for the lower Yalgorup Member in the central Block B.

6.1 Implication of fracture prediction for CO_2 storage

Fractures often occur in populations with power-law throw distributions with usually a higher frequency of small displacement faults and a lower frequency of large displacement faults (e.g. Ackermann et al., 2001, Meyer et al., 2002; Manzocchi et al., 2009). Observations of a restricted part of a fault population can be extrapolated to predict the range of unobserved faults in the same area (Yielding et al., 1996). Based on the available fault interpretation a preliminary cumulative frequency distribution of throw for the SW Hub is defined (Figure 30). This distribution suggests that the static geological model underestimates the number of faults with throw smaller than 120 m and that there could be as much as 300 faults with offset lower than the usual seismic resolution (between of 10 m to 20 m).

The fracture prediction for the SW Hub represents a first-order estimation of the distribution, orientation and initial mode of failure of these subseismic faults. Due to the limitations of the initial data (i.e., seismic faults distribution, geometry and offset, background strain and rock properties) and the lack of calibration data, the fracture prediction should primarily be used as a guide to understand and make first-order prediction on the detail small-scale deformation and estimate their potential impact on fluid flow within the reservoir and the top seal units. This could also be used to constrain the requirement for new data acquisition (e.g., type, location, density).

The modelled small-scale faults in the SW Hub are assumed to develop due to deformation controlled by stress perturbation around larger faults which is most likely caused by Early Cretaceous slip episodes. The ED models predict dominant initial shear failures with a maximum density in the central eastern part of Block B adjacent to F10 for both the Wonnerup Member and the Yalgorup Member and Eneabba Shale (Figure 25). Although the slip tendency values, based on the present-day in-situ stress data, are lower than the 0.6 threshold in Block B (Figures 27A and 28A), there is a relative increases of fracture predicted (near the maximum fracture density), near Harvey-1 and in the hanging wall compartment of F10, 8km southeast of Harvey-1 with values up to 0.3 for predicted fractures with dip >75° and NW orientations (Figure 29).

As already stated in section 5.3 the fracture stability is primarily controlled by depth variations and secondarily by fracture orientation. The fracture stability values for the modelled small faults are <10 MPa to the west of Block B where the Wonnerup and Yalgorup Members are the shallowest (Figure 28B). In the Timor Sea, Mildren et al. (2005) suggested a threshold of 10 MPa for the fracture stability below which

faults are likely to experience initial reactivation and to act as pathways for hydrocarbon over geological times. Applying this threshold to the small-scale shear faults predicted within the Yalgorup Member (Block B) would imply that the shear faults within c. 2km from fault F1 (footwall) might be at risk of creating pathways if they connect through the regional top seal (Figure 28B).

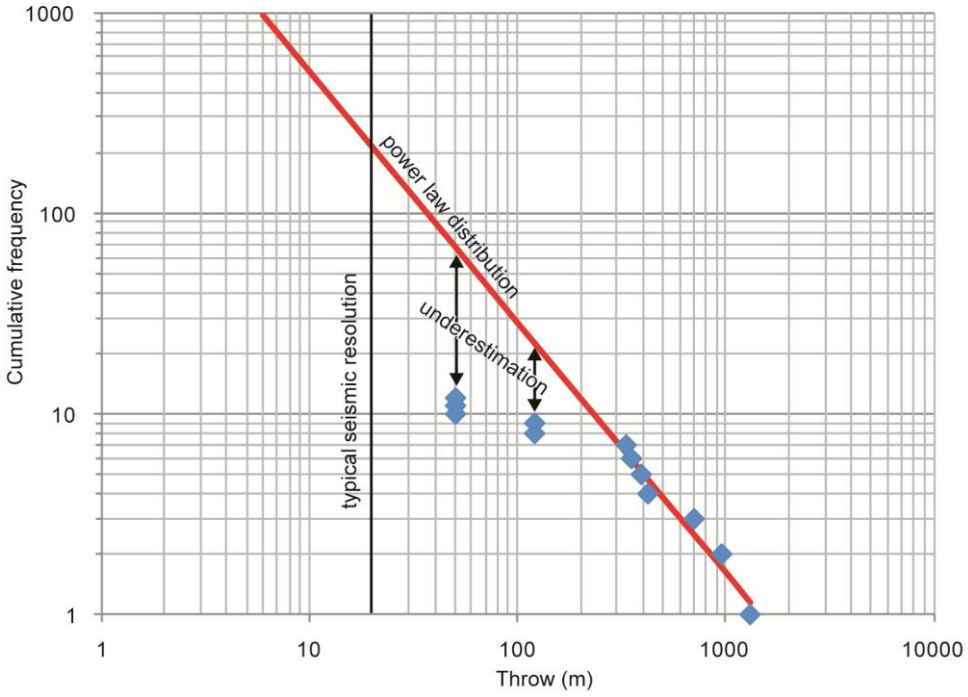

Figure 30: Preliminary cumulative frequency distribution of fault throw for the SW Hub. A power law distribution suggests that the number of interpreted faults with throw 120 m is underestimated.

7 Conclusions

To date, the available subsurface data from the SW Hub region present limitations and are not adequate to unambiguously image the stratigraphic and structural architectures and therefore the fault seal assessment represents only a guide for a first-order understanding of containment potential.

The CO_2 containment potential is largely controlled by fault hydraulic behaviour and can result in a risk of lateral migration of CO_2 (1) between reservoir compartments, (2) between reservoir and interbedded sandstone in the regional seal and (3) between reservoir and overburden and by (4) along fault migration of CO_2 between reservoir and overburden.

The limitations and the resulting uncertainties are:

- A low density of 2D seismic lines with an average spacing of 3km; this results in uncertainties on fault correlations, faults linkage, the definition of low displacement faults and the definition of the slip pattern on fault planes. We suggest that such a dataset allows only for the development of a regional first-order geological model that captures with a higher degree of confidence the structures with displacement >200m but that underestimates smaller structures.
- A sub-optimal distribution (i.e., location and orientation) of 2D seismic lines with mostly E-W and N-S oriented lines and a poor distribution to the SE of Block B and within Block A. This results in uncertainties on faults correlation, faults, the definition of low displacement faults and the definition of the slip pattern on fault planes as well as uncertainties on the stratigraphic horizons.
- Only one well (recently drilled Harvey-1) is reasonably tied to a seismic line in the Block B of the SW Hub. This greatly limits the development of a regionally meaningful 3D facies model. We suggest that only a first-order V_{sh} model can be derived directly from Harvey-1. For this reason we also used a forward stratigraphic model to explore depositional concepts in the SW V_{sh}sedsim in order to better capture the range of geological uncertainty.
- The absence of leak-off for the Leak-off test conducted in Harvey-1. The maximum and minimum horizontal stresses have to be defined using physically based relationships based on the frictional equilibrium criterion (Pevzner et al., 2013). This result is uncertainties on the in-situ stress field that affect the geomechanical fault seal assessment.
- The restricted geomechanical analysis performed on cores form Harvey-1. To date only 4 cores have been analysed for the Wonnerup Member. The rock properties for the Yalgorup Member are estimated from velocity data and initially calibrated with data from the Wonnerup Member. This leads to uncertainty in the geomechanical fault seal assessment and the sub-seismic fault prediction.

The regional first-order geological model is characterised by a N-S to NW-SE structural trend. The two main faults (N-S trending F1 and N-S to NNW-SSE trending F10) exhibit a maximum displacement of 900m and 1300m, respectively, and delimit three structural blocks (Blocks A, B and C) for the SW Hub. The Triassic and Jurassic horizons are dipping to the east.

The bounding fault between Blocks A and B (F10) is the only one that juxtaposes the Wonnerup with the overburden above the inferred regional seal. However SGR values on the fault plane are above 20% suggesting a reduced likelihood of across-fault migration and the supported CO_2 column before breaching the membrane seal is between 110 and 1100m. All the other faults define a juxtaposition seal (Wonnerup Member is juxtaposed against the Yalgorup Member and Eneabba shale) or a self-juxtaposition of the Wonnerup Member. The likelihood of lateral migration of CO_2 across faults between the Wonnerup Member and any interbedded sandstone (i.e., thief zones) in the Yalgorup Member can be locally high on

faults F1, F11 and 14. The likelihood of lateral migration across faults within the Wonnerup Member is high to average to the south of Block B with potential of westward migration from Block B to Block C if the CO_2 column exceeds the local offset of fault F1.

The main and subsidiary faults in Block B present an average to low likelihood of fault failure under the present-day stress (i.e., low likelihood to act as vertical pathways). The maximum CO_2 column height theoretically supported by a fault plane in the SW Hub is marginally orientation-dependant with slightly lower values for strike orientations between 50° and 160° (SE-NW to ENE-WSW) especially for fault with dip > 60°. However, depth has the most impact on the maximum supported column. An increasing depth results in an increase in stresses that will prevent failure to occur (i.e., on a Mohr Diagram a fault plane moves away from the failure envelop with increasing depth). The smallest CO_2 column heights required to reach failure stress are located to the north of Blocks A and B along faults F1, F2 and F10 and represent 1200 m or 1000 m of CO_2 when assuming a cohesive and cohesionless fault respectively. However, this smallest CO_2 column heights corresponds to fracture stability and slip stability values less than 10MPa and empirical data from Mildren et al. (2005) in the Timor Sea suggest that a pore pressure perturbation smaller than 10 MPa is likely to result in the initiation of hydrocarbon leakage over geological times (Figure 23). With the values for density and viscosity for supercritical CO_2 being similar to those of oil and gas we assume that the observation made by Mildren et al. (2005) for oil and gas field can be applied to CO_2 injection sites.

A statistical analysis of the interpreted fault population suggests that the geological model underestimates the number of faults with throw smaller than 120 m and that there could be as many as 300 faults with offset between of 10 m to 20 m. The fracture models, based on elastic dislocation theory, represents a first-order estimation of the distribution, orientation and initial mode of failure of the small-scale and subseismic faults that are predicted to have developed during the Early Cretaceous tectonic episode affecting the Wonnerup and the Yalgorup Members. The fracture models predict dominant shear failures with a maximum density in the central and eastern part of Block B adjacent to F10. The stress state of these small faults and fractures suggests that there is an average-low likelihood of failure under the present-day in-situ stress field in most past of Block B. The pore pressure increase required to reach failure stress decreases down to <10MPa to the west of Block B where the Wonnerup and Yalgorup Members are the shallowest. These values fall again below the empirical threshold from Mildren et al. (2005) and could suggest that shear faults within c. 2km from fault F1 (footwall) might be at risk of creating pathways if they connect through the regional top seal. With the values for density and viscosity for supercritical CO_2 being similar to those of oil and gas we assume that the observation made by Milder et al. (2005) for oil and gas field could be applied to CO_2 injection sites.

In light of these first-order assessments, the critical locations associated with higher risks for CO_2 containment in the SW Hub are:

- The south-western Block B with the possibility of lateral migration of CO_2 within the Wonnerup Member through F1 if the CO_2 column exceeds the local offset.
- The northern part of Block B with the possibility of vertical migration of CO_2 along faults F1, F2 and F10. However calibrations in the form of across-fault pressure differences, for instance, are still required to assess the presence of potential leak points.
- The central eastern Block B with the possibility of lateral migration of CO_2 between the Wonnerup Member and the Eneabba Formation. However, additional stratigraphic data to constrain the volume of phyllosilicates and additional calibrations in the form of across-fault pressure differences are required to assess the presence of potential leak points.

In order to gain more understanding on the hydraulic behaviour of faults the following locations for additional wells are proposed (Figure 31):

- On the hanging-wall and footwall of F10 (A and B in Figure 31). A well in the hanging-wall (A in Figure 31) will test the presence of higher fracture density in the Wonnerup and Yalgorup Members. It could also validate the presence of better Wonnerup reservoir (Griffith et al., 2012). A

well in the footwall (B in Figure 31) could be used to test across-fault pressure difference pre- and/or post injection. Both well will bring valuable improvement in the facies model and fractures definition.

- On the hanging-wall and footwall of F1 (C and D in Figure 31). A well in the hanging-wall (C in Figure 31) will test the presence of critically-stressed fracture in the Wonnerup and Yalgorup Members (Figure 27Figure 28). A well in the footwall (D in Figure 31) could be used to test across-fault pressure difference pre- and/or post injection. Both well will bring valuable improvement in the facies model and fractures definition.

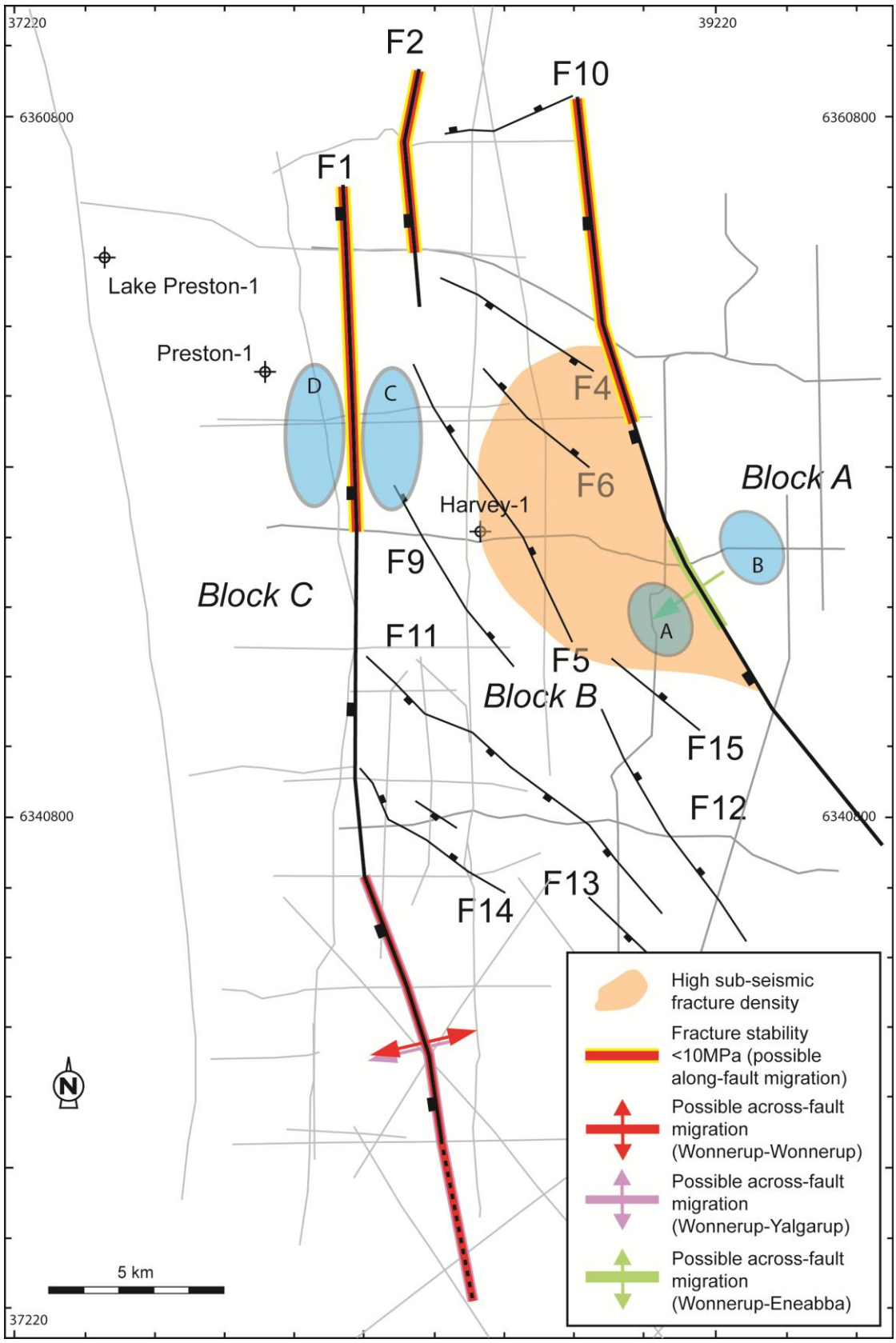

Figure 31: Locations of proposed additional wells (in blue). See Section 7 for discussion.

8 Recommendations

In light of the first-order assessment of the CO_2 containment for the SW Hub it is recommended to:

- Acquire additional subsurface data, especially seismic reflection data in order to decrease uncertainties on the subsurface architecture and constrain the structural framework, i.e., the definition/calibration of fault orientation, fault linkage, fault relay and small-scale faults. This is critical to further evaluate the distribution of potential leak points. 3D seismic reflection data over at least one of the block bounding fault would greatly improve the understanding in major faults geometry and slip history.
- Constrain the local stratigraphic framework by increasing the regional stratigraphic correlation and acquiring additional data to calibrate the models of phyllosilicates distribution (V_{sh}) and the distribution of geomechanical and petrophysical properties. This is critical to further evaluate the distribution of reservoirs and seals, to constrain the membrane seal capacity of faults and to predict small-scale fault distribution and failure mode. Denser seismic and stratigraphic data should be used to define the relationship between acoustic impedance and V_{sh} and carry out seismic inversion and further investigate the spatial variation of the V_{sh}.
- Constrain the in-situ stress field.
- Acquire pressure data on fault compartments to constrain the across-fault pressure difference and calibrate the membrane fault seal calculations.
- Sample fault zones (cores) and define the geomechanical and petrophysical properties of faults to constrain the geomechanical fault seal assessment.

Additionally, for a more comprehensive assessment of CO_2 storage potential it must be demonstrated that the mechanical effects of CO_2 injection and storage will not cause the deterioration of the mechanical stability and the isolation capacity of the sequestration site. It is therefore critical to further assess the effect of induced stress changes by coupling :

- Thermal-multiphase fluid flow simulations to estimate the distribution and magnitude of pore pressure build-up and thermal effects due to CO_2 injection,
- Geomechanical-multiphase fluid flow simulations to investigate the poro-mechanical effects caused by pressure build-up and thermal contraction due to CO_2 injection and risk of top seal and fault failures through time,
- Chemical-geomechanical simulations to investigate the interaction between CO_2-rich fluids and top seal mineralogy, the resulting effects on rocks mechanical behaviour and the impacts on top seal integrity trough time.

References

ABRAMS, M. A., 1996. DISTRIBUTION OF SUBSURFACE HYDROCARBON SEEPAGE IN NEAR-SURFACE MARINE SEDIMENTS: AAPG MEMOIR 66, 1–14.

ACKERMANN, R.V., SCHLISCHE, R.W., WITHJACK, M.O., 2001. THE GEOMETRIC AND STATISTICAL EVOLUTION OF NORMAL FAULT SYSTEMS: AN EXPERIMENTAL STUDY OF THE EFFECTS OF MECHANICAL LAYER THICKNESS ON SCALING LAWS. JOURNAL OF STRUCTURAL GEOLOGY 23, 1803–1819.

AL-CHALABI, M., 1994, SEISMIC VELOCITIES - A CRITIQUE, FIRST BREAK, 12, NO.12, 589-596.

ALLAN, U.S. 1989. MODEL FOR HYDROCARBON MIGRATION AND ENTRAPMENT WITHIN FAULTED STRUCTURES. AAPG BULLETIN, 73, 803–811.

ANDERSON, R., FLEMINGS, P., LOSH, S., AUSTIN, J., WOODHAMS, R., 1994. GULF OF MEXICO GROWTH FAULT DRILLED, SEEN AS OIL, GAS MIGRATION PATHWAY: OIL & GAS JOURNAL, 92, 97–104.

ANTONELLINI, M., AYDIN, A., 1994. EFFECT OF FAULTING ON FLUID FLOW IN POROUS SANDSTONES: PETROPHYSICAL PROPERTIES: AAPG BULLETIN, V. 78, P. 355– 377.

ASQUITH, G. AND KRYGOWSKI, D., 2004. GAMMA RAY, IN ASQUITH, G. AND KRYGOWSKI, D. BASIC WELL LOG ANALYSIS: AAPG METHODS IN EXPLORATION 16, P.31-35.

BARTON C.A., ZOBACK, M.D., MOOS, D., 1995. FLUID-FLOW ALONG POTENTIALLY ACTIVE FAULTS IN CRYSTALLINE ROCK: GEOLOGY, 23, 913-916.

BOURNE, S. J., WILLEMSE, E. J. M., 2001. ELASTIC STRESS CONTROL ON THE PATTERN OF TENSILE FRACTURING AROUND A SMALL FAULT NETWORK AT NASH POINT, UK. JOURNAL OF STRUCTURAL GEOLOGY, 23, 1753–1770.

BOURNE, S. J., RIJKELS, L., STEPHENSON, B. J., WILLEMSE, E. J. M., 2001. PREDICTIVE MODELLING OF NATURALLY FRACTURED RESERVOIRS USING GEOMECHANICS AND FLOW SIMULATION. GEOARABIA, 6, 27–42.

BOUVIER, J.D., KAARS-SIJPESTEIJN, C.H., KLUESNER, D.F., ONYEJEKWE, C.C., VAN DER PAL, R.C. 1989. THREE-DIMENSIONAL SEISMIC INTERPRETATION AND FAULT SEALING INVESTIGATIONS, NUN RIVER FIELD, NIGERIA. AAPG BULLETIN, 73, 1397–1414.

BRADSHAW, J., RIGG, A., 2001. THE GEODISC PROGRAM: RESEARCH INTO GEOLOGICAL SEQUESTRATION OF CO_2 IN AUSTRALIA. ENVIRONMENTAL GEOSCIENCES, 8, 3, 166–176.

BRETAN, P., YIELDING, G., JONES, H., 2003. USING CALIBRATED SHALE GOUGE RATIO TO ESTIMATE HYDROCARBON COLUMN HEIGHTS. AAPG BULLETIN, 87, 397–413.

BRETAN, P., YIELDING, G., MATHIASSEN, O.M., THORSNES, T., 2011. FAULT-SEAL ANALYSIS FOR CO_2 STORAGE: AN EXAMPLE FROM THE TROLL AREA, NORWEGIAN CONTINENTAL SHELF. PETROLEUM GEOSCIENCE,. 17 2011, 181–192.

BYERLEE, J. D., 1978. FRICTION OF ROCK. PURE & APPLIED GEOPHYSICS, 116, 615–626.

CARTWRIGHT, J., HUUSE, M., APLIN, A., 2007. SEAL BYPASS SYSTEMS: AAPG BULLETIN, V. 91, 1141-1166.

CAUSEBROOK, R., DANCE, T., BALE, K., 2006. SOUTHERN PERTH BASIN SITE INVESTIGATION AND GEOLOGICAL MODEL FOR STORAGE OF CARBON DIOXIDE. CO2CRC REPORT NUMBER: RPT06-0162.

CHIARAMONTE, L., ZOBACK, M.D., FRIEDMANN, J., STAMP, V., 2008. SEAL INTEGRITY AND FEASIBILITY OF CO_2 SEQUESTRATION IN THE TEAPOT DOME EOR PILOT: GEOMECHANICAL SITE CHARACTERIZATION. ENVIRONMENTAL GEOLOGY, 54, 1667–1675.

CHILDS, C., WATTERSON, J., WALSH, J.J. 1997. COMPLEXITY IN FAULT ZONE STRUCTURE AND IMPLICATIONS FOR FAULT SEAL PREDICTION. IN: MØLLER-PEDERSEN, P. & KOESTLER, A.G. (EDS) HYDROCARBON SEALS: IMPORTANCE FOR EXPLORATION AND PRODUCTION. NORWEGIAN PETROLEUM SOCIETY (NPF) SPECIAL PUBLICATION, ELSEVIER, SINGAPORE, 7, 61–72.

CIFTCI, B.N., LANGHI, L., STRAND, J., S GOLDIE-DIVKO, L., MIRANDA. J., O'BRIEN, G., 2012. TOP SEAL BYPASS RISK DUE TO FRACTURE SYSTEMS, NEARSHORE/ONSHORE GIPPSLAND BASIN. THE APPEA JOURNAL AND CONFERENCE PROCEEDINGS, 52, 397-413.

COCKBAIN, A.E., 1990. PERTH BASIN, GEOLOGY AND MINERAL RESOURCES OF WESTERN AUSTRALIA, GEOLOGICAL SURVEY OF WESTERN AUSTRALIA, MEMOIR 3, 495-524.

CROSTELLA, A., BACKHOUSE, J., 2000. GEOLOGY AND PETROLEUM EXPLORATION OF THE CENTRAL AND SOUTHERN PERTH BASIN, WESTERN AUSTRALIA. GEOLOGICAL SURVEY OF WESTERN AUSTRALIA REPORT 57.

CROUCH, S. L., STARFIELD, A. M., 1983. BOUNDARY ELEMENT METHODS IN SOLID MECHANICS: WITH APPLICATIONS IN ROCK MECHANICS AND GEOLOGICAL ENGINEERING. ALLEN AND UNWIN, WINCHESTER, MA.

DANIEL, R.F., KALDI, J.G., 2008. EVALUATING SEAL CAPACITY OF CAPROCKS AND INTRAFORMATIONAL BARRIERS FOR THE GEOSEQUESTRATION OF CO_2. PESA EASTERN AUSTRALIAN BASINS SYMPOSIUM III, 475–484

DEE, S. J., YIELDING, G., FREEMAN, B. HEALY, D., KUSZNIR, N. J., GRANT, N., ELLIS, P., 2007. ELASTIC DISLOCATION MODELLING FOR PREDICTION OF SMALL-SCALE FAULT AND FRACTURE NETWORK CHARACTERISTICS. IN LONERGAN, L., JOLLY, R. J. H., RAWNSLEY, K. & SANDERSON, D. J. (EDS) FRACTURED RESERVOIRS. GEOLOGICAL SOCIETY, LONDON, SPECIAL PUBLICATIONS, 270, 139–155.

DELLE PIANE, C., OLIEROOK, H.K.H., TIMMS, N.E., SAEEDI, A., ESTEBAN, L., RAZAEE, R., MIKHALTSEVITCH, V., AND LEBEDEV, M., 2013, FACIES-BASED ROCK PROPERTIES DISTRIBUTION ALONG THE HARVEY 1 STRATIGRAPHIC WELL, CSIRO REPORT NUMBER EP133710.

DEWHURST, D. N., AND R. M. JONES, 2002. GEOMECHANICAL, MICROSTRUCTURAL AND PETROPHYSICAL EVOLUTION IN EXPERIMENTALLY REACTIVATED CATACLASITES: APPLICATION TO FAULT SEAL PREDICTION: AAPG BULLETIN, V. 86, 1383–1405.

DEWHURST, D.N., JONES, M.R., HILLIS, R. R., MILDREN, S.D., 2002. MICROSTRUCTURAL AND GEOMECHANICAL CHARACTERISATION OF FAULT ROCKS FROM THE CARNRVON AND OTWAY BASINS: AUSTRALIAN PETROLEUM PRODUCTION AND EXPLORATION ASSOCIATION JOURNAL, 42, 167–186.

ETRIS, E.L., CRABTREE, N.J., DEWAR, J., PICKFORD, S., 2001. TRUE DEPTH CONVERSION: MORE THAN A PRETTY PICTURE. CSEG RECORDER (NOVEMBER), 11-22.

FAIRBRIDGE, R. W., 1953. AUSTRALIAN STRATIGRAPHY: PERTH. UNIVERSITY OF WESTERN AUSTRALIA TEXT BOOKS BOARD, 516P.

FERRILL, D.A., WINTERLE, J., WITTMEYER, G., SIMS, D., COLTON, S., ARMSTRONG, A., MORRIS, A.P., 1999. STRESSED ROCK STRAINS GROUNDWATER AT YUCCA MOUNTAIN NEVADA. GSA TODAY, 9, 1–8.

FINKBEINER, T., ZOBACK, M., FLEMINGS, P. B., STUMP, B. B., 2000. STRESS, PORE PRESSURE, AND DYNAMICALLY CONSTRAINED HYDROCARBON COLUMNS IN THE SOUTH EUGENE ISLAND 330 FIELD, NORTHERN GULF OF MEXICO: AAPG BULLETIN, V. 85, 1007–1031.

FISHER, Q.J., KNIPE, R.J., 1998. FAULT SEALING PROCESSES IN SILICICLASTIC SEDIMENTS. IN: G. JONES, Q.J. FISHER AND R.J. KNIPE (EDITORS), FAULTING, FAULT SEALING AND FLUID FLOW IN HYDROCARBON RESERVOIRS. GEOL. SOC., LONDON, SPEC. PUBL., 147, 117–134.

FREEMAN, B., YIELDING, G., NEEDHAM, D.T., BADLEY, M.E., 1998. FAULT SEAL PREDICTION: THE GOUGE RATIO METHOD. IN: COWARD, M.P., DALTABAN, T.S. & JOHNSON, H. (EDS) STRUCTURAL GEOLOGY IN RESERVOIR CHARACTERIZATION. GEOLOGICAL SOCIETY, LONDON, SPECIAL PUBLICATIONS, 127, 19–25.

FRISTAD, T., GROTH, A., YIELDING, G., FREEMAN, B. 1997. QUANTITATIVE FAULT SEAL PREDICTION: A CASE STUDY FROM OSEBERG SYD. IN: MØLLER-PEDERSEN, P. & KOESTLER, A.G. (EDS). HYDROCARBON SEALS: IMPORTANCE FOR EXPLORATION AND PRODUCTION. NORWEGIAN PETROLEUM SOCIETY (NPF) SPECIAL PUBLICATION, ELSEVIER, SINGAPORE, 7, 107–124.

FULLJAMES, J.R., ZIJERVELD, L.J.J., FRANSSEN, R.C.M.W. 1997. FAULT SEAL PROCESSES: SYSTEMATIC ANALYSES OF FAULT SEALS OVER GEOLOGICAL AND PRODUCTION TIMESCALES. IN: MØLLER-PEDERSEN, P. & KOESTLER, A.G. (EDS) HYDROCARBON SEALS: IMPORTANCE FOR EXPLORATION AND PRODUCTION. NORWEGIAN PETROLEUM SOCIETY (NPF) SPECIAL PUBLICATION, ELSEVIER, SINGAPORE, 7, 51–59.

GARTRELL, A. P., LISK, M., 2005. POTENTIAL NEW METHOD FOR PALEOSTRESS ESTIMATION BY COMBINING 3D FAULT RESTORATION AND FAULT SLIP INVERSION TECHNIQUES: FIRST TEST ON THE SKUA FIELD, TIMOR SEA, IN P. BOULT AND J. K. KALDI, EDS., EVALUATING FAULT AND CAP ROCK SEALS: AAPG HEDBERG SERIES 2, 23–36.

GIBSON, R.G., 1994. FAULT-ZONE SEALS IN SILICICLASTIC STRATA OF THE COLUMBUS BASIN, OFFSHORE TRINIDAD. BULL. AM. ASSOC. PET. GEOL., 78: 1372–1385.

GRASSO, J. R., 1992. MECHANICS OF SEISMIC INSTABILITIES INDUCED THE RECOVERY OF HYDROCARBONS. PURE & APPLIED GEOPHYSICS, 139, 507–534.

GRIFFITHS, C. M., DYT, C., 2001. SIX YEARS OF SEDSIM EXPLORATION APPLICATIONS (ABSTRACT ONLY), AAPG BULLETIN, 85 (2001), 13.

GRIFFITHS, C. M.,PARASCHIVOIU, E., 1998. THREE-DIMENSIONAL FORWARD STRATIGRAPHIC MODELLING OF EARLY CRETACEOUS SEDIMENTATION ON THE LEVEQUE AND YAMPI SHELVES, BROWSE BASIN. APPEA JOURNAL, 38 (1), 147-158.

GRIFFITHS, C., DYT, C., PARASCHIVOIU, E., LIU, K., 2001. SEDSIM IN HYDROCARBON EXPLORATION. IN: MERRIAM, D. AND DAVIS, J. (EDS.), GEOLOGIC MODELLING AND SIMULATION. KLUWER ACADEMIC, NEW YORK, 71–97.

GRIFFITHS, C. M., SEYEDMEHDI, Z., SALLES, T., DYT, C., 2012. STRATIGRAPHIC FORWARD MODELLING FOR SOUTH WEST COLLIE HUB PHASE ONE - STATIC MODEL. ANLEC R&D PROJECT *7-0411-0129;* CSIRO REPORT NUMBER EP13068.

IASKY, R. P., 1993. A STRUCTURAL STUDY OF THE SOUTHERN PERTH BASIN, WESTERN AUSTRALIA: WESTERN AUSTRALIA GEOLOGICAL SURVEY REPORT 31, 1993, 56P.

IASKY, R. P., LOCKWOOD, A. M., 2004. GRAVITY AND MAGNETIC INTERPRETATION OF THE SOUTHERN PERTH BASIN, WESTERN AUSTRALIA. WESTERN AUSTRALIA GEOLOGICAL SURVEY, RECORD 2004/8, 32P.

JAEGER, J. C., COOK, N. G. W., 1979. FUNDAMENTALS OF ROCK MECHANICS. CHAPMAN & HALL, NEW YORK, 76P.

JENNINGS, J.B., 1987. CAPILLARY PRESSURE TECHNIQUES: APPLICATION TO EXPLORATION AND DEVELOPMENT GEOLOGY. AAPG BULLETIN, 71, 1196–1209.

JEV, B.I., KAARS-SIJPESTEIJN, C.H., PETERS, M.P.A.M, WATTS, N.L., WILKIE, J.T. 1993. AKASO FIELD, NIGERIA: USE OF INTEGRATED 3D SEISMIC, FAULT SLICING, CLAY SMEARING, AND RFT PRESSURE DATA ON FAULT TRAPPING AND DYNAMIC LEAKAGE. AAPG BULLETIN, 77, 1389–1404.

JONES, R. M., D. N., DEWHURST, R. R. HILLIS, S. D. MILDREN, 2002. GEOMECHANICAL FAULT CHARACTERIZATION: IMPACT ON QUANTITATIVE FAULT SEAL RISKING. SOCIETY OF PETROLEUM ENGINEERS/INTERNATIONAL SOCIETY FOR ROCK MECHANICS ROCKMECHANICS CONFERENCE, IRVING, TEXAS, OCTOBER 2002: SPE PAPER 78213.

KALUZA, M. J., DOYLE, E. H., 1996. DETECTING FLUID MIGRATION IN SHALLOW SEDIMENTS, CONTINENTAL SLOPE ENVIRONMENT, GULF OF MEXICO: AAPG MEMOIR 66, 15–26.

KNIPE, R. J., 1992. FAULTING PROCESS AND FAULT SEAL, IN R. M. LARSON, H. BREKE, B. T. LARSEN, AND E. TALLERAAS, EDS., STRUCTURAL AND TECTONIC MODELLING AND ITS APPLICATION TO PETROLEUM GEOLOGY: NORWEGIAN PETROLEUM SOCIETY SPECIAL PUBLICATION 1, STAVANGER, P. 325– 342.

KNIPE R. J., FISHER, Q. J., JONES, M. R., CLENNELL, M. B., FARMER, A., HARRISON, B., KIDD, E., MCALISTER, E., PORTER, J. R., WHITE, E. A., 1997. FAULT SEAL ANALYSIS: SUCCESSFUL METHODODLOGIES, APPLICATION AND FUTURE DIRECTIONS, IN P. MOELLER-PEDERSEN, AND A.G. KOESTLER, EDS., HYDROCARBON SEALS: IMPORTANCE FOR EXPLORATION AND PRODUCTION: NORWEGIAN PETROLEUM SOCIETY SPECIAL PUBLICATIONS 7, 15-40.

KNIPE, R.J., JONES, G., FISHER, Q.J. 1998. FAULTING, FAULT SEALING AND FLUID FLOW IN HYDROCARBON RESERVOIRS: AN INTRODUCTION. IN: JONES, G., FISHER, Q.J. & KNIPE, R.J. (EDS) FAULTING, FAULT SEALING AND FLUID FLOW IN HYDROCARBON RESERVOIRS. GEOLOGICAL SOCIETY, LONDON, SPECIAL PUBLICATIONS, 147, VII–XXI.

KOLTERMANN, C. E., GORELICK, S. M., 1992. PALAEOCLIMATIC SIGNATURE IN TERRESTRIAL FLOOD DEPOSITS. SCIENCE, 256 (5065), 1775-1782.

LANGHI, L., ZHANG, Y., GARTRELL, A., UNDERSCHULTZ, J.R., DEWHURST, D.N., 2010. EVALUATING HYDROCARBON TRAP INTEGRITY DURING FAULT REACTIVATION USING GEOMECHANICAL 3D MODELLING: AN EXAMPLE FROM THE TIMOR SEA, AUSTRALIA. AAPG BULLETIN 94, 567-591.

LE BLANC SMITH, G., 1993. GEOLOGY AND PERMIAN COAL RESOURCES OF THE COLLIE BASIN, WESTERN AUSTRALIA. WESTERN AUSTRALIA GEOLOGICAL SURVEY, REPORT 38, 86P.

LI, F., DYT, C., GRIFFITHS, C.M., JENKINS, C., RUTHERFORD, M., CHITTLEBOROUGH, J., 2005. SEABED SEDIMENT TRANSPORT AND OFFSHORE PIPELINE RISKS IN THE AUSTRALIAN SOUTHEAST. APPEA JOURNAL 45, 523-534.

LIGTENBERG, J. H., 2005. DETECTION OF FLUID MIGRATION PATHWAYS IN SEISMIC DATA: IMPLICATIONS FOR FAULT SEAL ANALYSIS. BASIN RESEARCH 17, 141–153.

LISLE, R.J., SRIVASTAVA, D.C., 2004. TEST OF THE FRICTIONAL REACTIVATION THEORY FOR FAULTS AND VALIDITY OF FAULT-SLIP ANALYSIS. GEOLOGY 32 (7), 569–572.

MAERTEN, L., GILLESPIE, P., POLLARD, D. D., 2002. EFFECTS OF LOCAL STRESS PERTURBATION ON SECONDARY FAULT DEVELOPMENT. JOURNAL OF STRUCTURAL GEOLOGY, 24, 145–153.

MANZOCCHI, T., WALSH, J.J., BAILEY, W.R., 2009.POPULATION SCALING BIASES IN MAP SAMPLES OF POWER-LAW FAULT SYSTEMS. JOURNAL OF STRUCTURAL GEOLOGY, 31, 12, 1612–1626.

MARTINEZ, P., HARBAUGH, J. W., 1993. SIMULATING NEARSHORE ENVIRONMENTS. PERGAMON PRESS, NEW YORK.

MEYER, V., NICOL, A., CHILDS, C., WALSH, J.J., WATTERSON, J., 2002. PROGRESSIVE LOCALISATION OF STRAIN DURING THE EVOLUTION OF A NORMAL FAULT SYSTEM. JOURNAL OF STRUCTURAL GEOLOGY 24, 1215–1231.

MEYER, M., HARFF, J., DYT, C., 2011. MODELLING COASTLINE CHANGE OF THE DARSS-ZINGST PENINSULA WITH SEDSIM. (IN J. HARFF ET AL. (EDS.)), THE BALTIC SEA BASIN, CENTRAL AND EASTERN EUROPEAN DEVELOPMENT STUDIES , (CEEDES) 2011, PART 5, 281-298, DOI: 10.1007/978-3-642-17220-5_14

MILDREN, S.D., HILLIS, R.R., DEWHURST, D.N., LYON, P.J., MEYER, J.J., BOULT, P.J., 2005. FAST: A NEW TECHNIQUE FOR GEOMECHANICAL ASSESSMENT OF THE RISK OF REACTIVATION-RELATED BREACH OF FAULT SEALS. IN: BOULT, P. & KALDI, J. (EDS) EVALUATING FAULT AND CAP ROCK SEALS. AAPG HEDBERG SERIES, 2, 73–85.

MOECK, I., GRZEGORZ, K., ZIMMERMANN, G., 2009. SLIP TENDENCY ANALYSIS, FAULT REACTIVATION POTENTIAL AND INDUCED SEISMICITY IN A DEEP GEOTHERMAL RESERVOIR. JOURNAL OF STRUCTURAL GEOLOGY 31, 1174–1182.

MORRIS, A., FERRILL, D.A., HENDERSON, D.B., 1996. SLIP TENDENCY ANALYSIS AND FAULT REACTIVATION. GEOLOGY 24 (3), 275–278.

MORY, A. J., IASKY, R. P., 1996. STRATIGRAPHY AND STRUCTURE OF THE ONSHORE NORTHERN PERTH BASIN, WESTERN AUSTRALIA. WESTERN AUSTRALIA GEOLOGICAL SURVEY, REPORT 46, 101P.

MUIR-WOOD, R., KING G.C.P., 1993. HYDROLOGICAL SIGNATURES OF EARTHQUAKE STRAIN: JOURNAL OF STRUCTURAL GEOPHYSICAL RESEARCH-SOLID EARTH, 98, 22035-22068.

MYERS, J.S., HOCKING, R.M., 1998. GEOLOGICAL MAP OF WESTERN AUSTRALIA, 1:2,500,000, 13TH ED. WESTERN AUSTRALIA GEOLOGICAL SURVEY.

NICHOLSON, C.J., BORISSOVA, I.,KRASSAY, A.A., BOREHAM, C.J., MONTEIL, E., NEUMANN, V., DI PRIMIO, R., BRADSHAW, B.E., 2008. NEW EXPLORATION OPPORTUNITIES IN THE SOUTHERN VLAMING SUB-BASIN. THE APPEA JOURNAL AND CONFERENCE PROCEEDINGS, 48, 371-380.

O'BRIEN, G. W., LISK, M., DUDDY, I. R., HAMILTON, J., WOODS, P., COWLEY, R., 1999. PLATE CONVERGENCE, FORELAND DEVELOPMENT AND FAULT REACTIVATION, PRIMARY CONTROLS ON BRINE MIGRATION, THERMAL HISTORIES AND TRAP BREACH IN THE TIMOR SEA, AUSTRALIA: MARINE AND PETROLEUM GEOLOGY, 16, 6, 533–560

OKADA, Y., 1985. SURFACE DEFORMATION DUE TO SHEAR AND TENSILE FAULTS IN A HALF-SPACE. BULLETIN OF THE SEISMOLOGICAL SOCIETY OF AMERICA, 75, 1135–1154.

OKADA, Y., 1992. INTERNAL DEFORMATION DUE TO SHEAR AND TENSILE FAULTS IN A HALF-SPACE. BULLETIN OF THE SEISMOLOGICAL SOCIETY OF AMERICA, 82, 1018–1040.

PEVZNER, R., LUMLEY, D., UROSEVIC, M., GUREVICH, B., BÓNA, A., ALAJMI, M.A., SHRAGGE, J., PERVUKHINA, M., MUELLER, T., SHULAKOVA, V., 2013. ADVANCED GEOPHYSICAL DATA ANALYSIS AT HARVEY-1: STORAGE SITE CHARACTERIZATION AND STABILITY ASSESSMENT. ANLEC R&D PROJECT NUMBER 7-1111-0198.

RALEIGH, C.B., HEALY, J.H., BREDEHOFFT, J.D., 1976. AN EXPERIMENT IN EARTHQUAKE CONTROL AT RANGELEY, COLORADO. SCIENCE 191:1230–1237.

REVIL, A., CATHLES III, L. M., 2002. FLUID TRANSPORT BY SOLITARY WAVES ALONG GROWING FAULTS. A FIELD EXAMPLE FROM THE SOUTH EUGENE ISLAND BASIN, GULF OF MEXICO. EPSL 202, 321-335.

RUTQVIST, J., BIRKHOLZER, J., CAPPA, F., TSANG, C.F., 2007. ESTIMATING MAXIMUM SUSTAINABLE INJECTION PRESSURE DURING GEOLOGICAL SEQUESTRATION OF CO_2 USING COUPLED FLUID FLOW AND GEOMECHANICAL FAULT-SLIP ANALYSIS. ENERGY CONVERSION AND MANAGEMENT, 48, 1798–1807.

SALLES, T. B., GRIFFITHS, C. M., DYT, C.P., 2011B. AEOLIAN SEDIMENT TRANSPORT INTEGRATION IN GENERAL STRATIGRAPHIC FORWARD MODELLING. JGR/186062, JOURNAL OF GEOLOGICAL RESEARCH. JOURNAL OF GEOLOGICAL RESEARCH, VOL. 2011, ARTICLE ID 186062, 12 PAGES.

SALLES, T. B., GRIFFITHS, C. M., DYT, C.P., LI, F., 2011A. AUSTRALIAN SHELF SEDIMENT TRANSPORT RESPONSES TO CLIMATE CHANGE-DRIVEN OCEAN PERTURBATIONS. MARINE GEOLOGY 282, 268–274.

SALLES, T., MARCHES, E., DYT, C., GRIFFITHS, C., HANQUIEZ, V., MULDER, T., 2009. SIMULATION OF THE INTERACTIONS BETWEEN GRAVITY PROCESSES AND CONTOUR CURRENTS ON THE ALGARVE MARGIN (SOUTH PORTUGAL) USING THE STRATIGRAPHIC FORWARD MODEL SEDSIM. SEDIMENTARY GEOLOGY, 229, 3, 95–109.

SANDERSON, D. J., AND X. ZHANG, 1999. CRITICAL STRESS LOCALIZATION OF FLOW ASSOCIATED WITH DEFORMATION OF WELL-FRACTURED ROCK MASSES, WITH IMPLICATIONS FOR MINERAL DEPOSITS: GEOLOGICAL SOCIETY (LONDON) SPECIAL PUBLICATION 155, 69–81.

SECOR, D.T., 1965. ROLE OF FLUID PRESSURE IN JOINTING. AM J. SCI 263, 633-646.

SECOR, D.T., 1969. MECHANICS OF NATURAL EXTENSION FRACTURING AT DEPTH IN THE EARTH'S CRUST. PAP. GEOL., SURV. CAN., 68-52, 3-48.

SMITH, D. A., 1966. THEORETICAL CONSIDERATIONS OF SEALING AND NONSEALING FAULTS: AAPG BULLETIN 50, 363-374.

SIBSON, R.H. 1987. EARTHQUAKE RUPTURING AS A HYDROTHERMAL MINERALIZING AGENT. GEOLOGY 15, 701-704.

SIBSON, R. H., 1996. STRUCTURAL PERMEABILITY OF FLUID-DRIVEN FAULT-FRACTURE MESHES. JOURNAL OF STRUCTURAL GEOLOGY 18, 1031–1042.

SORKHABI, R., TSUJI, Y., 2005. THE PLACE OF FAULTS IN PETROLEUM TRAPS, IN R. SORKHABI AND Y. TSUJI, EDS., FAULTS, FLUID FLOW AND PETROLEUM TRAPS: AAPG MEMOIR 85, 1-31.

STREIT, J.E. AND HILLIS, R.R. 2004. ESTIMATING FAULT STABILITY AND SUSTAINABLE FLUID PRESSURES FOR UNDERGROUND STORAGE OF CO_2 IN POROUS ROCK. ENERGY, 29, 1445–1456.

TETZLAFF, D. M.,HARBAUGH, J. W., 1989. SIMULATING CLASTIC SEDIMENTATION; COMPUTER METHODS IN THE GEOSCIENCES, VAN NOSTRAND REINHOLD, NEW YORK, 202.

UNDERSCHULTZ, J., 2007. HYDRODYNAMICS AND MEMBRANE SEAL CAPACITY: GEOFLUIDS, 7, 148-158.

VAN RUTH P J. 2006. GEOMECHANICS: VLAMING SUB-BASIN, WESTERN AUSTRALIA. CO2CRC REPORT NUMBER RPT06-0043.

VARMA, S., UNDERSCHULTZ, J., DANCE, T., LANGFORD, R., ESTERLE, J., DODDS, K. AND VAN GENT, D., 2009. REGIONAL STUDY ON POTENTIAL CO_2 GEOSEQUESTRATION IN THE COLLIE BASIN AND THE SOUTHERN PERTH BASIN OF WESTERN AUSTRALIA. MARINE AND PETROLEUM GEOLOGY. V26. P 1255-1273.

WATTS, N.L. 1987. THEORETICAL ASPECTS OF CAP-ROCK AND FAULT SEALS FOR SINGLEAND TWO PHASE HYDROCARBON COLUMNS. MARINE AND PETROLEUM GEOLOGY, 4, 274–307.

WILKES, P., TIMMS, N., HOROWITZ, F., CORBEL, S., 2011. A NEW STRUCTURAL INTERPRETATION OF THE PERTH BASIN AND THE PERTH METROPOLITAN AREA USING GRAVITY AND AEROMAGNETIC DATA, GEOMORPHOLOGY AND GEOLOGY. WESTERN AUSTRALIA GEOTHERMAL CENTRE OF EXCELLENCE REPORT NO EP117411, 65P.

WILKINS S. J., NARUK S. J., 2007, QUANTITATIVE ANALYSIS OF SLIP-INDUCED DILATION WITH APPLICATION TO FAULT SEAL. AAPG BULLETIN, V. 91, 97–113.

WIPRUT, D., ZOBACK, M.D., 2000. FAULT REACTIVATION AND FLUID FLOW ALONG A PREVIOUSLY DORMANT NORMAL FAULT IN THE NORTHERN NORTH SEA. GEOLOGY, 28, 595-598.

YIELDING, G. 2002. SHALE GOUGE RATIO – CALIBRATION BY GEOHISTORY. IN: KOESTLER, A.G. & HUNSDALE, R. (EDS) HYDROCARBON SEAL QUANTIFICATION NORWEGIAN PETROLEUM SOCIETY (NPF) SPECIAL PUBLICATION, ELSEVIER, AMSTERDAM, 11, 1–15.

YIELDING, G., FREEMAN, B., NEEDHAM, T., 1997. QUANTITATIVE FAULT SEAL PREDICTION. AAPG BULLETIN, 81, 897–917.

YIELDING, G., NEEDHAM, T., JONES, H., 1996. SAMPLING OF FAULT POPULATIONS USING SUB-SURFACE DATA: A REVIEW. JOURNAL OF STRUCTURAL GEOLOGY, VOLUME 18, ISSUES 2–3, 135-146.

ZOBACK, M. (ED.) 2007. RESERVOIR GEOMECHANICS, CAMBRIDGE UNIVERSITY PRESS, 448 P.

ZOBACK, M. D., TOWNEND, J., 2001. IMPLICATIONS OF HYDROSTATIC PORE PRESSURES AND HIGH CRUSTAL STRENGTH FOR THE DEFORMATION OF INTRAPLATE LITHOSPHERE. TECTONOPHYSICS, 336, 19–30.

CONTACT US

t 1300 363 400
+61 3 9545 2176
e enquiries@csiro.au
w www.csiro.au

FOR FURTHER INFORMATION

CESRE
Laurent Langhi
t +61 8 6436 8741
e laurent.langhi@csiro.au

YOUR CSIRO

Australia is founding its future on science and innovation. Its national science agency, CSIRO, is a powerhouse of ideas, technologies and skills for building prosperity, growth, health and sustainability. It serves governments, industries, business and communities across the nation.